Overview of changes to the model and the manuscript

Both the underlying formulation of the model and its presentation have been extensively reworked in response to the reviewers' comments. We think the paper is much improved and we are grateful to the reviewers for their time and insights.

The kinetics of Hg transformation have been revised, with the largest changes specifically to the pathways for demethylation and the rate of gas exchange. Now the processes of biological degradation of MMHg, producting Hg(II), is distinct in the model from photodegradation, which we treat as a reduction following Bergquist and Blum. In the previous version of the manuscript these were combined, both forming Hg(0), and we reported that changing that combined pathway to produce Hg(II) would alter the Δ^{199}Hg of the Hg^{tot} in the entire ocean. Now that we resolve the distinction between biological and photochemical degradation of MMHg, the issue we reported in the first version has disappeared; either version of the photochemical reaction seems to work in reproducing the isotopic signature observed in surface waters.

Reviewer #1 was disappointed that we didn't "game out" the kinetics models more thoroughly, and in response we have done a suite of sensitivity studies of the Hg speciation in the ocean in response to uncertainties in 10 different kinetic rate constants.

We compare our model results with observational data in this version of the manuscript – both concentration data and the Δ^{199}Hg of monomethyl Hg inferred from fish data. Reviewer #1 was correct when pointing out that the concentrations in our deep ocean were too high. It turned out to be caused by an error in the gas exchange coefficient, now fixed, with the high sensitivity of the deep ocean Hg concentration to the gas exchange coefficient documented in the sensitivity section.

An issue that we had previously with the adsorption constant for Hg onto POC has also been resolved (Reviewer #1 caught it, again). The units that are used to report the adsorption of Hg onto particles are somewhat strange, requiring POC to be in units of kg/L.

We have added the Δ^{200}Hg isotopic system to the simulation, which appears to be a recorder of the relative rates of wet and dry Hg deposition, with perhaps the potential to resolve differences between basins in this ratio.

The advantage of the HAMOCC code is that it is fast enough to do many studies. We believe the paper now makes better use of this strength, by presenting many sensitivity runs, to particle sinking rate, the adsorption constant, kinetic rate parameters, and isotopic fractionation mechanisms.

Responses to specific reviewer comments – Reviewer #1

Page 3: on subsurface interconversion between Hg(II) and Hg(0); this is included in the model, as it also was in the previous version. There was a confusing sentence in the manuscript, now gone, which seemed to imply to the reviewer that there was no interconversion between Hg(II) and Hg(0) in subsurface waters, but what the sentence was trying to say was that photochemical reactions only happen in surface waters.

Page 7: The section on method limitations has been clarified.

Page 8: The section from the previous manuscript about MMHg production in low-O2 conditions has been removed, replaced with the kinetics sensitivity studies. O2 in HAMOCC is problematic in that it goes slightly negative in the equatorial Pacific, and our previous formulation of just increasing MMHg production rates when O2 goes low was too simple. Rather than show the MMHg sensitivity to an unrealistic kinetics change, better to show profiles of all Hg species as they respond to many different kinetics changes.

Page 9 Line 2, "there are some regional variations in Hg, but they are not systematic, as compared to the clear Pac-Atl differences exhibited by nutrient-type elements..." Not true...the Lamborg 2014 paper specifically made the counter argument. The distribution of Hg is the nutrient like distribution with a transient anthropogenic signal superimposed.

That sentence referred to a scenario with only advection, no particles. In Figure 2 one can see a nutrient-type distribution of deep Hg in the full model, as a function of the sinking rate of particles. Looking at the data, however, there are a lot of high values in the North Atlantic, so the nutrient-type distribution is not totally clear.

Section 3.3, this first paragraph is written in a way that's a bit hard to follow.

This section is one of several in the paper that has been extensively rewritten; we hope it is clearer now.

Page 10: added reference to Medina et al paper submitted to *Global Biogeochemical Cycles* that includes measurements of Δ^{199}Hg of Hg(II) on particles. There is also a new figure comparing the model results with those observations.

Figure 6 and 9: A sentence has been added explaining the point of figure 6, and the previous figure 9 has been subsumed into figure 3, but the point of it is also explained in the text.

Figure 11-15 and isotopic data. We have added a comparison with MMHg Δ^{199}Hg measurements from fish, and we show profiles, maps, and summaries, in the hopes of showing patterns that people could look for in new measurements.

Reviewer #2

Comments and suggestions by reviewer #2 were extremely useful and helpful, and were pretty much entirely adopted in the text.

Figure 6 now has data and other model results for comparison.

A model of mercury cycling and isotopic fractionation in the ocean

David E. Archer[1], Joel D. Blum[2]

[1]Department of the Geophysical Sciences, University of Chicago, Chicago, 60637, USA
[2]Department of Earth and Environmental Sciences, University of Michigan, Ann Arbor, Michigan 48109

Correspondence to: David E. Archer (d-archer@uchicago.edu)

Abstract. Mercury speciation and isotopic fractionation processes have been incorporated into the HAMOCC offline ocean tracer advection code. The model is fast enough to allow a wide exploration of the sensitivity of the Hg cycle in the oceans, and of factors controlling human exposure to monomethyl-Hg through the consumption of fish. Vertical particle transport of Hg appears to play a discernable role in setting present-day Hg distributions, which we surmise by the fact that in simulations without particle transport, the high present-day Hg deposition rate leads to an Hg maximum at the sea surface, rather than a subsurface maximum as observed. Hg particle transport has a relatively small impact on anthropogenic Hg uptake, but it sequesters Hg deeper in the water column, so that excess Hg is retained in the model ocean for a longer period of time after anthropogenic Hg deposition is stopped. Among 10 rate constants in the model, steady state Hg concentrations are most sensitive to reactions that are sources or sinks of Hg(0), the evasion of which to the atmosphere is the dominant sink term in the surface ocean. Isotopic fractionations in the interconversion reactions are most strongly expressed, in the isotopic signatures of dissolved Hg, in reactions that involve the dominant dissolved species, Hg(II), including mass independent fractionation during Hg photoreduction. The Δ^{199}Hg of MMHg in the model, subject to photoreduction fractionation, reproduces the Δ^{199}Hg of fish in the upper 1000 m of the ocean, while the impact of anthropogenic Hg deposition on Hg isotope ratios is essentially negligible.

1 Background

The element mercury (Hg) is a powerful neurotoxin and has no known use or function in metabolism (Clarkson and Magos, 2006). When transformed to methyl mercury (MeHg) it is known to amplify its toxicity by bio-accumulating up the food chain. The main human exposure to MeHg is via consumption of high trophic level seafood (Chen et al., 2016;Schartup et al., 2018). Humans have been mining and mobilizing Hg into the Earth surface environment for hundreds of years, as a by-product of coal combustion, and for its use in gold mining, and in products such as electronics and light bulbs (Amos et al., 2013;Driscoll et al., 2013;Krabbenhoft and Sunderland, 2013;Lamborg et al., 2014;Obrist et al., 2018;Streets et al., 2017;Mason et al., 2012). The Hg load in the surface ocean has increased by a factor of 3-5 since the industrial revolution; this represents a massive human impact on the global Hg cycle (Streets et al., 2017).

david archer 8/21/2018 8:55 AM
Style Definition ... [2]
david archer 8/21/2018 8:55 AM
Style Definition ... [1]
david archer 8/21/2018 8:55 AM
Deleted: Hg via
david archer 8/21/2018 8:55 AM
Deleted: incorporation into
david archer 8/21/2018 8:55 AM
Deleted: only
david archer 8/21/2018 8:55 AM
Deleted: The concentration of monomethyl ... [3]
david archer 8/21/2018 8:55 AM
Deleted: , with model experiments suggesti ... [4]
david archer 8/21/2018 8:55 AM
Deleted: could have as significant an impac ... [5]
david archer 8/21/2018 8:55 AM
Deleted: simulated, independently and com ... [6]
david archer 8/21/2018 8:55 AM
Deleted: predict their expression in the spa ... [7]
david archer 8/21/2018 8:55 AM
Deleted: in the
david archer 8/21/2018 8:55 AM
Deleted: .
david archer 8/21/2018 8:55 AM
Deleted: ,
david archer 8/21/2018 8:55 AM
Deleted: ,
david archer 8/21/2018 8:55 AM
Deleted: fundamentally toxic to our metabo ... [8]
david archer 8/21/2018 8:55 AM
Deleted: It
david archer 8/21/2018 8:55 AM
Deleted: the only heavy metal
david archer 8/21/2018 8:55 AM
Deleted: magnify
david archer 8/21/2018 8:55 AM
Deleted: , and the
david archer 8/21/2018 8:55 AM
Deleted: Hg
david archer 8/21/2018 8:55 AM
Deleted: which accumulates Hg from the ocean
david archer 8/21/2018 8:55 AM
Deleted: thousands
david archer 8/21/2018 8:55 AM
Deleted: ;

Hg can be extremely mobile in the environment, with gaseous forms in the atmosphere, and with particle-reactive forms allowing it to travel through soils and rivers and into the oceans (Fitzgerald et al., 2007). Hg(II) has a high affinity for complexing with (or adsorbing to) sulfur-rich ligands in organic matter (Schartup et al., 2015), and this leads to Hg accumulation with organic carbon in soils (Amos et al., 2013;Smith-Downey et al., 2010;Biswas et al., 2008) and sediments (Hollweg et al., 2010). The high mobility of Hg implies that the amount of Hg in earth surface reservoirs is transient, even in the steady-state pre-human Hg cycle (Amos et al., 2013), and that Hg can be potentially mobilized by human impacts such as the thawing of Arctic permafrost (Schuster et al., 2018;Obrist et al., 2017) or enhanced wildfire activity (Turetsky et al GRL 2006).

The Hg cycle is analogous to the carbon cycle, in which fossil fuel extracted from the solid Earth is released to a fast surface system consisting of soils and oceans in communication via the atmosphere. In both cases, the long-term sink for the perturbation is burial in sediments of the ocean. Because these burial fluxes are relatively slow, it will take a long time for these perturbations to subside: thousands of years for the Hg cycle (Amos et al., 2013), and hundreds of thousands of years for the carbon cycle (Archer et al., 2009). Other forms of environmental degradation that will persist for thousands of years include actinide radioactive waste, and some anthropogenic gases such as sulfur hexafluoride (Ray et al., 2017).

It is extremely challenging to predict the future of human exposure to Hg, because the Hg cycle is so complex (Blum, 2013). One challenge has been to characterize the quantitative role of Hg adsorbed onto sinking particles in the ocean (Lamborg et al., 2016), which will constrain how deeply anthropogenic Hg may have penetrated into the ocean (Lamborg et al., 2014;Munson et al., 2015;Zhang et al., 2014b). Another is to understand the factors that control the production of MeHg, which is the bio-accumulating form but which comprises only a small fraction of the Hg in the ocean (Schartup et al., 2015;Schartup et al., 2013;Ortiz et al., 2015;Lehnherr et al., 2011;Lehnherr, 2014;Jonsson et al., 2016;Chakraborty et al., 2016;Blum et al., 2013).

Stable isotopes provide a powerful tool for determining the origins (Kwon et al., 2014;Li et al., 2014;Sherman et al., 2015;Sherman et al., 2013;Balogh et al., 2015;Demers et al., 2015;Donovan et al., 2014;Donovan et al., 2013;Gehrke et al., 2011;Sun et al., 2016;Tsui et al., 2014;Sonke JE, 2010;Yin R, 2013) and transformations (Kwon et al., 2013;Kwon et al., 2014;Rodriguez-Gonzalez et al., 2009;Chandan et al., 2015;Yang and Sturgeon, 2009;Foucher D, 2013;Jiskra M, 2012), of Hg in the natural environment. Hg has seven stable isotopes with six at high abundance (>1%). Most chemical processes fractionate the various isotopes progressively according to their masses (Mass Dependent Fractionation, MDF). If all fractionation processes were strictly mass dependent, measurements of the proportions of more than two isotopes would be redundant information. However, Hg is susceptible to light-stimulated reactions, which include oxidation of Hg(0) and reduction of Hg(II) and MeHg. These photochemical reactions exhibit MDF and Mass Independent Fractionation (MIF), which distinguishes between isotopes beyond their mass differences (Blum et al., 2014;Bergquist and Blum, 2009). Odd mass number mass independent fractionations, or (odd-MIF), are produced by two mechanisms. Large magnitude effects (>~0.4‰) are seen in kinetic short-lived radical pair reactions and are believed to be caused by the magnetic isotope effect (Buchachenko, 2001;Bergquist and Blum, 2009). Smaller magnitude even-MIF can also be produced during dark

david archer 8/21/2018 8:55 AM
Deleted: long-lived…aseous forms in the g ... [9]

david archer 8/21/2018 8:55 AM
Deleted: material mined…ossil fuel extrac ... [10]

david archer 8/21/2018 8:55 AM
Deleted: rich and…complex (Blum, 2013 ... [11]

david archer 8/21/2018 8:55 AM
Deleted: (… ADDIN EN.CITE (Kwon et ... [12]

david archer 8/15/2018 1:14 PM
Comment [1]: Reviewer #2 wrote a snotty comment here: "Might it be that other groups than the group also published interesting papers on Hg isotopes?" so I threw in a bunch more papers, unfortunately you're still a coauthor on many of them so I guess we're just screwed.

david archer 8/21/2018 8:55 AM
Deleted: (<…>1%). Most chemical proce ... [13]

equilibrium reduction and oxidation reactions by the nuclear volume effect (Schauble, 2007;Zheng and Hintelmann, 2010). Even-MIF has been observed in Hg in the atmosphere (Gratz et al., 2010) and deposited from atmospheric sources (Strok et al., 2015;Zheng et al., 2016), and is believed to occur in the tropopause, but the specific mechanism is not known (Chen et al., 2012). Mass independent fractionation provides multiple degrees of freedom, allowing measurements of the proportions of all the isotopes to carry much more information than would be possible if only MDF occurred.

We have incorporated a model of the chemical transformations and isotopic fractionations of Hg in the ocean into the HAMOCC offline ocean passive tracer advection model (Maier-Reimer and Hasselmann, 1987). The flow field is taken from the Large Scale Geostrophic (LSG) dynamics model, which is also extremely fast and efficient for 3-D ocean flow (Maierreimer et al., 1993). The LSG physical model takes a time step of a month by eliminating non-geostrophic parts of the circulation that would be violated by this extremely long time step. The HAMOCC tracer advection model takes an annual average flow field from 12 monthly time steps of the LSG model and uses it to advect tracers through the ocean. While the tracers are flowing, they exchange with the atmospheric gases (in the case of CO_2 and O_2), and with biota (as CO_2, O_2, alkalinity, and nutrients).

The distribution of Hg in the ocean today is the product of a presumably steady state natural Hg cycle, which takes thousands of years to achieve in the model due to the ocean turnover time, followed by a global human perturbation which began in about 1850 (and which could persist for thousands of years into the future). HAMOCC is believed to still be the fastest off-line 3-D ocean tracer advection code in existence, and is ideal for studying the sensitivity of the ocean Hg cycle on these long time scales. This paper is also the first attempt in our knowledge to simulate the isotopic fractionation processes of Hg in the ocean, which take thousands of years to express themselves globally.

david archer 8/21/2018 8:55 AM
Deleted: . But the large magnitude (>~0.4‰) odd MIF is only from photochemical processes. ... [14]

david archer 8/21/2018 8:55 AM
Deleted: Hamocc…AMOCC offline ocean ... [15]

david archer 8/21/2018 8:55 AM
Deleted: an extreme… global human pertu ... [16]

2 Modeling Methods

2.1 Mercury Geochemistry Solvers

The geochemical cycling of Hg in the ocean in Hg-HAMOCC is similar in conception to previous models (Figure 1). Hg interconverts between Hg(II), Hg(0), monomethyl-Hg (MMHg), dimethyl-Hg (DMHg), and Hg adsorbed to sinking particles (Hg-P). The rates of the biological reactions are correlated to each other and to the overall rate of metabolic activity in the (Semeniuk and Dastoor, 2017) model and in our model, with typical values as shown in Figure 1. The rate constant for MMHg production from Hg(II) is proportional to the rate of POC degradation, which is derived from the attenuation with depth of the sinking POC flux in HAMOCC (expressed as a volumetric rate of POC degradation).

Other Hg transformation reactions are provoked by light, and only take place in the surface ocean (Blum et al., 2014;Bergquist and Blum, 2007). The rate of photochemical reactions in Hg-HAMOCC is about a factor of two higher in low versus high latitudes, using the latitudinal function that governs export production rates in HAMOCC. The photochemical reaction rates are attenuated with water depth, using an e-folding depth scale of 20 meters. The wavelength dependence of photochemical reactions and fractionations is complex (Rose et al., 2015), and the attenuation depth of the

david archer 8/21/2018 8:55 AM
Deleted: (Semeniuk and Dastoor, 2017;Zhang et al., 2014) (but with modifications as described in Results section) …Figure 1). Hg interconve ... [17]

david archer 8/21/2018 8:55 AM
Deleted: near…n the surface ocean (Blum ... [18]

light varies with frequency, so the 100 m depth scale is only an approximation. The actual mechanisms for DMHg production and degradation are still uncertain, so the model formulation can be regarded as something of placeholder for the time being. The rates of gas evasion of Hg(0) and DMHg are taken to be proportional to the concentrations of the species. The Hg cycle in the surface ocean is driven by deposition influx of Hg(II) and gas invasion of Hg(0), which are applied at uniform rates around the world.

All of the rate constants in Hg-HAMOCC are first-order, which is to say that the chemical rates are determined by multiplying the rate constant by a single species concentration to the first power. Rates of conversion between these species are generally fast, some much faster than the 1-year time step of the tracer code. For this reason, solvers were written to find steady state distributions of the Hg species. Because the Hg system is strongly driven at the sea surface by air-sea fluxes, a separate solver system was developed for surface grid points than the one applied to subsurface grid points.

Export of sinking Hg-P is done separately from the speciation calculations in subsurface waters, but simultaneously with the speciation calculations in the surface ocean. Hg advection by ocean circulation is also done in an independent step from the chemistry and particle components. Since the Hg speciation is imposed to be at equilibrium by the speciation solvers, there is no need to carry speciation information through the advective system, which only needs to carry around a single tracer for the total Hg concentration. To treat the isotopic systematics of the Hg cycle, we added three additional advected Hg tracers, identical to the first but with slightly altered source fluxes or rate constants, in order to simulate variations in the relative abundances of isotopes ^{199}Hg, ^{200}Hg, and ^{202}Hg relative to ^{198}Hg.

2.1.1 Surface ocean chemistry solver

For the surface ocean, the distribution of Hg among the dissolved species is determined by a balance of Hg fluxes through the system: rain input of Hg(II) and Hg(0), and removal by Hg(II) scavenging on sinking particles and degassing as Hg(0) and DMHg. Concentration-dependent reaction rates in the model are all assumed to be first-order, i.e. linear in Hg concentration. This includes loss by gas evasion, which should be linear in Hg concentration in the piston velocity model, and loss of bound Hg on sinking particles, which is linear with [Hg(II)] in the adsorption model. The solver finds values for the Hg species concentrations at which the incoming and loss fluxes balance. The equations are:

$$\begin{bmatrix} -k_{20}-k_{2M}-k_{2D}-S & k_{02} & k_{M2} & 0 \\ k_{20}+k & -k_{evp}-k_{02} & k_{M0} & 0 \\ k_{2M} & 0 & -k_{M2}-k_{M0}-k_{MD} & k_{DM} \\ k_{2D} & 0 & k_{MD} & -k_{evp}-k_{DM} \end{bmatrix} \begin{bmatrix} [Hg(2+)] \\ [Hg(0)] \\ [MMHg] \\ [DMHg] \end{bmatrix} = \begin{bmatrix} -Dep_{Hg(2+)} \\ 0 \\ 0 \\ -Dep_{Hg(0)} \end{bmatrix}$$

where k denotes a first-order rate constant, subscripts denote reactant then product where 2 = Hg(II), 0 = Hg(0), D = DMHg, and M = MMHg. The Dep terms on the right-hand side denote deposition from the atmosphere at fixed imposed rates. S is a rate constant for Hg(II) sinking on particles

david archer 8/21/2018 8:55 AM
Deleted: 50m

david archer 8/21/2018 8:55 AM
Deleted: .

david archer 8/21/2018 8:55 AM
Formatted: Font color: Auto

Joel Blum 8/4/2018 1:18 PM
Comment [2]: since we don't know anything about DMHg isotopes we could assume it all degrades to MMHg?? OK No Problem.

david archer 8/2/2018 1:28 PM
Comment [3]: But since it's a gas we know it will evade, and that alternative pathway has interesting impacts on the isotopes, and anyway everything would have to be re-done to take it out. Which I could do easily, it's all automated, if there were a strong reason to.

david archer 8/21/2018 8:55 AM
Deleted: , on the assumption that atmospheric concentrations are negligible…. The Hg ... [19]

david archer 8/21/2018 8:55 AM
Deleted: has

Joel Blum 8/4/2018 1:22 PM
Comment [4]: I think this is OK, but how ... [20]

david archer 8/21/2018 8:55 AM
Deleted: two…hree additional advected H ... [21]

Joel Blum 5/15/2018 2:24 PM
Comment [5]: why not carry the delta va ... [22]

Joel Blum 7/31/2018 1:57 PM
Comment [6]: I don't understand howyo ... [23]

david archer 8/21/2018 8:55 AM
Deleted: 2+),…I) and Hg(0), and removal ... [24]

Joel Blum 5/15/2018 2:39 PM
Comment [7]: as we discussed could add ... [25]

david archer 8/21/2018 8:55 AM
Deleted: . Since Hg degassing and sinkin ... [26]

Joel Blum 7/31/2018 2:12 PM
Comment [8]: change Hg(2+) in Figure to Hg(0)

david archer 8/21/2018 8:55 AM
Deleted:
$$\begin{bmatrix} -k_{20}-k_{2M}-k_{2D}-S & k_{02} \\ k_{20} & -k_{evp} \\ k_{2M} & 0 \\ k_{2D} & 0 \end{bmatrix}$$

david archer 8/21/2018 8:55 AM
Deleted: 2+),…I), 0 = Hg(0), D = DMHg, ... [27]

$$S = \left(1 - \frac{1}{k_b[POC]+1}\right)\frac{R}{dz}$$

comprised of the POC concentration, the scavenging constant, and an imposed POC sinking velocity R. The diagonal terms in the first matrix represent sinks of the chemical species listed in the second matrix, when those sinks are calculated as the rate constants in the diagonal multiplied by the species concentration (which is solved for). The positive off-diagonal terms in the first matrix represent sources of species, which are calculated as rate constants times the concentration of the origin species. This linear algebraic calculation solves for the steady-state concentrations of the four Hg species without iteration (in contrast to an analogous solver in HAMOCC for CO_2 system chemistry).

2.1.2 Subsurface ocean chemistry solver

The Hg cycle in the deep ocean differs from that of the surface in that fluxes of Hg into and out of the system (by desorption of Hg(II) from particles) are slow relative to the rates of interconversion between the Hg species. Because all of the rate constants are first-order, the relative proportions of the species are independent of the total Hg concentration. The solver finds steady state values of all species relative to that of Hg(II), then scales everything to fit the total Hg concentration as produced by the advection routine. The equations are:

$$\begin{bmatrix} -k_{02} & k_{M2} & 0 \\ 0 & -k_{M0}-k_{M2}-k_{MD} & k_{DM} \\ 0 & k_{MD} & -k_{DM} \end{bmatrix} \begin{bmatrix} [Hg(0)] \\ [MMHg] \\ [DMHg] \end{bmatrix} = \begin{bmatrix} -1pM \times k_{20} \\ -1pM \times k_{2M} \\ -1pM \times k_{2D} \end{bmatrix}$$

where a concentration of 1pM is assumed for [Hg(II)], in order to work out the relative proportions of the other species. After the proportions of all the species concentrations are worked out, they are scaled to match the total Hg concentration as it is slowly changed by advection and desorption from POC. Maps of Hg total concentration are compared with measurements in Figure 2, and profiles of the Hg species are shown in Figure 3. In addition to the global mean, profiles from the highly productive equatorial Pacific to the oligotrophic Atlantic are shown to span the range of variability in the model.

2.2 Hg adsorption and transport on particles

Hg has a strong chemical affinity for organic matter, in particular for organic sulfur ligands. This chemistry leads Hg to adsorb onto organic matter in the ocean, leading to a vertical sinking flux of adsorbed Hg on particles (Lamborg et al., 2016). Characterizing this flux is complicated by the fact that sinking particles compete for Hg with suspended and dissolved organic carbon (Han et al., 2006;Fitzgerald et al., 2007).

david archer 8/21/2018 8:55 AM
Deleted: the assumed

david archer 8/21/2018 8:55 AM
Deleted: Nonzero terms in the right-hand matrix represent fixed-rate sources, of which deposition of Hg(2+) is the only example.

david archer 8/21/2018 8:55 AM
Formatted: Subscript

david archer 8/21/2018 8:55 AM
Deleted: 2+)

david archer 8/21/2018 8:55 AM
Deleted: Hg2+,

david archer 8/21/2018 8:55 AM
Deleted: $\begin{bmatrix} -k_{02} & k_{M2} & 0 \\ 0 & -k_{M0} & k_{DM} \\ 0 & k_{MD} & -k_{DM} \end{bmatrix} \begin{bmatrix} [\\ [M \\ [D \end{bmatrix}$

david archer 8/21/2018 8:55 AM
Deleted: 2+)],

david archer 8/21/2018 8:55 AM
Deleted: Profiles

david archer 8/21/2018 8:55 AM
Deleted: , in the Atlantic and Pacific,

david archer 8/21/2018 8:55 AM
Deleted: 2. The locations are chosen

david archer 8/21/2018 8:55 AM
Deleted: span

david archer 8/21/2018 8:55 AM
Deleted: range of variability in the model,

david archer 8/21/2018 8:55 AM
Deleted: The human biological impacts of

david archer 8/21/2018 8:55 AM
Deleted: occur because of the

david archer 8/21/2018 8:55 AM
Deleted: of Hg

david archer 8/21/2018 8:55 AM
Deleted: to

david archer 8/21/2018 8:55 AM
Deleted: The same

The biological pump in HAMOCC is represented as an instantaneous vertical redistribution of nutrients and other associated biological elements, without ever resolving them into particles or tracking their sinking. We constructed a hypothetical POC profile from this functioning of HAMOCC by choosing a POC sinking velocity that would transform the export production from the euphotic zone in HAMOCC into surface POC concentrations that are close to the observed mean concentration of about 5 μM. This sinking velocity of 500 meters per year is much slower than the 100 meters per day inferred sinking velocities of the particles that carry the bulk of the material caught in sediment traps, but it is similar to that used by other recent estimates (Semeniuk and Dastoor, 2017;Lamborg et al., 2016), and comparable to the result of modeling thorium on particles (Anderson et al., 2016), which (similarly to Hg) binds to both suspended and sinking particles. Because POC in the real ocean spans in size from dissolved to fast-sinking, the imposition of a single velocity in the model formulation, to be applied to the entire adsorbed Hg pool, is an oversimplification of reality, and the velocity required for the best fit is not a simple thing that can be measured directly in the real ocean. The sensitivity of the model to the sinking velocity is shown in Figure 4. With an increase in sinking velocity, the "biological pump" for Hg becomes stronger, increasing the concentration in the deep ocean. The scavenging lifetime of Hg decreases as the sinking flux increases with increasing sinking velocity. When the Hg sinking velocity is set to 500 m/yr, the same velocity as is used to transform the POC flux into a POC concentration, the global Hg sinking rate is similar to the result of Semeniuk and Dastoor (2017) (Figure 5). However, sinking fluxes of Hg in the mid water column are about a factor of three lower than equatorial and North Pacific sediment trap fluxes from Munson et al. (2015), so the models could be under-predicting the real particle fluxes if the Munson et al. (2015) data are globally representative. The turnover time of dissolved Hg, with respect to transiting through the water column on sinking particles, depends on the sinking velocity, as shown in Figure 4. Values approaching 1000 years in the deep ocean have been reported in other models (Semeniuk and Dastoor, 2017;Zhang et al., 2014a), and imply that circulation plays a major role in determining deep ocean Hg concentrations.

A second degree of freedom in the system of sinking Hg on particles is the adsorption constant K_d, defined such that:

$$[\text{Hg-P}] / [\text{Hg(II)}] = K_d\,[\text{POC}] \qquad \text{(eqn. 1)}$$

Semeniuk and Dastoor (2017) and Zhang et al. (Zhang et al., 2014a) used a value of $2 \cdot 10^5$, in units of L kg^{-1} (requiring POC to be in kg L^{-1}), but included a factor of 10 correction for the fraction of particulate material in the ocean that is organic carbon ("f_{oc}"), resulting in an effective K_d of $2 \cdot 10^6$. Lamborg et al. (2016) derived a value of about $4 \cdot 10^6$, which they claim to be a factor of 20 higher than the value used in the models, but after the f_{oc} correction in the models the values only differ by a factor of 2. The data from Bowman et al. (2015), analysed by Lamborg et al. (2016), showed that about 5% of the Hg(II) in surface waters is bound to sinking particles, similar to the results from the models (Semeniuk and Dastoor, 2017). A map of the bound fraction in surface waters from our model is shown in Figure 6, showing more particulate Hg in high-production (high POC) regions such as the equatorial Pacific. The sensitivity of the model to the value of K_d is shown in Figure 4, with results similar to those for sinking velocity. The calculated lifetime of dissolved Hg in the water column, relative to removal by adsorption to sinking particles, is shown in Figure 7. The figure is intended for comparison with results of other models,

david archer 8/21/2018 8:55 AM
Deleted: Hamocc

david archer 8/21/2018 8:55 AM
Deleted: micromolar

david archer 8/21/2018 8:55 AM
Deleted: 2

david archer 8/21/2018 8:55 AM
Deleted: day

david archer 8/21/2018 8:55 AM
Deleted: actual

david archer 8/21/2018 8:55 AM
Deleted: of about 100 meters per day,

david archer 8/21/2018 8:55 AM
Deleted: . ... [28]

david archer 8/21/2018 8:55 AM
Moved down [1]: (2016) derived a value of about $4 \cdot 10^6$,

david archer 8/21/2018 8:55 AM
Deleted: a factor of 20 higher. The preferred value of K_d in our formulation is $1 \cdot 10^4$, which is 20 times lower than the Semeniuk

david archer 8/21/2018 8:55 AM
Moved down [2]: (2017)

david archer 8/21/2018 8:55 AM
Deleted: value. The target of our tuning of K_d was to reproduce the salient result from the model of Semeniuk (2017) and the data from Lamborg (2016) that about 5% of the Hg(2+) in surface waters is bound to sinking particles (Figure 3). The huge differences must arise due to differences in t ... [29]

david archer 8/21/2018 8:55 AM
Deleted: underpredicting

david archer 8/21/2018 8:55 AM
Deleted: particles

david archer 8/21/2018 8:55 AM
Deleted: .

david archer 8/21/2018 8:55 AM
Deleted: 6

david archer 8/21/2018 8:55 AM
Deleted: 2014

david archer 8/21/2018 8:55 AM
Deleted: ,

david archer 8/21/2018 8:55 AM
Deleted:

david archer 8/21/2018 8:55 AM
Moved (insertion) [2]

david archer 8/21/2018 8:55 AM
Moved (insertion) [1]

and to show that the Hg cycle in the ocean is close to a crossover point between dominance by fluid advection vs. sinking particles.

2.3 Isotopic fractionation

Mercury isotope fractionations associated with any of the processes in the Hg cycle are treated in the model as kinetic effects, slight perturbations in the rates of chemical transformations between the isotopes (rather than fractionation of the equilibrium state). This allows Hg-HAMOCC to impose fractionation effects onto the kinetic expressions in the solvers for surface and subsurface Hg speciation. The altered kinetic rate constants are applied to alternative total Hg concentration fields representing the isotopes ^{199}Hg, ^{200}Hg, and ^{202}Hg relative to a "base" isotope ^{198}Hg. For many processes, such as advection by fluid flow and mixing, isotopic delta values can be manipulated directly as a tracer. However, to calculate the expression of an isotope fractionation in the steady state solution to a web of chemical reactions requires that we simulate the impact of the fractionation on the budgets of the different isotopes, as the simplest way to come up with a delta value.

The way that the model treats the isotopes differs from reality, for a numerical convenience, following a trick developed by Ernst Maier-Reimer in HAMOCC many years ago for carbon isotope ratios (Maier-Reimer, 1984). In the real world, the total Hg concentration is comprised of multiple isotopes. In the model, the concentrations of Hg in the ocean are taken as that of a base isotope. Then the entire Hg cycle in the model is duplicated, and the kinetic constants slightly altered, to represent the behaviour of a different Hg isotope. Each isotopic field corresponds to how the total Hg field would behave if it were entirely comprised of its particular Hg isotope, subject to slightly altered sources and kinetic rate constants for that isotope.

The deviations of the fields for the other isotopes are represented as ratios relative to the base field, and presented in permil (‰), where the ratio of the "standard" is 1 rather than the particular ratio of the isotopic reference standard for natural samples. The relative differences, represented as ratios in ‰, are the same between variations in the isotopes in reality and between the altered fields in the model, even though the concentrations are different between the two cases. The advantage of this scheme is that the fields representing the different isotopes are subjected to similar computational rounding errors, because their values are similar. Also it is simpler to simulate the behaviour of total Hg in a single field, rather than as a more complicated sum of isotopic concentrations as in reality.

Because the chemical speciation of Hg is solved for each time step, there is no need to advect the concentrations of chemical species such as MMHg. The advection scheme in the model carries the total concentrations representing each isotope. Each isotope field is divided into the different Hg species assuming steady state and using the web of kinetic rate constants appropriate to that isotope. The slightly altered speciation of one isotope relative to another, and the slightly differing sources and sinks for that isotope, lead to slight differences between the abundances of each isotope overall in the Hg pool.

Mass-dependent fractionation processes are imposed on all isotopic systems, with the rates depending on how much heavier an isotope is than mass 198. Mass-independent fractionations in the ocean are applied only to the ^{199}Hg system, while the ^{200}Hg system is driven only by different isotopic signatures of wet (Hg(II)) vs. dry (Hg(0)) deposition. Mass independent

david archer 8/21/2018 8:55 AM
Deleted: Potential isotopic

david archer 8/21/2018 8:55 AM
Deleted: :

david archer 8/21/2018 8:55 AM
Deleted: at

david archer 8/21/2018 8:55 AM
Deleted: kinetics

Joel Blum 8/4/2018 2:29 PM
Comment [9]: can you say something about 198Hg just to satisfy readers curiosity?

david archer 8/21/2018 8:55 AM
Deleted: styled after even and odd

david archer 8/21/2018 8:55 AM
Deleted: of Hg, specifically,

david archer 8/21/2018 8:55 AM
Deleted: . The MIF fractionation only applies to odd ^{199}Hg, whereas MDF processes apply to both isotopes, with an impact roughly 4 times stronger for mass 202 than for 199 (

david archer 8/21/2018 8:55 AM
Deleted: 198). As for isotopic measurements in reality, the MIF component of the fractionation is isolated by subtracting from the measured d199 value the expected MDF based on the δ^{202} value, to produce a composite quantity Δ^{199}. As was done

david archer 8/21/2018 8:55 AM
Deleted: , it is helpful in the model to set the nominal computational

david archer 8/21/2018 8:55 AM
Deleted: the three isotopes equal, rather than at some artibrary ratio as

david archer 8/21/2018 8:55 AM
Deleted: nature,

david archer 8/21/2018 8:55 AM
Deleted: minimize

david archer 8/21/2018 8:55 AM
Deleted: . The delta values are insensitive to this convenience,

david archer 8/21/2018 8:55 AM
Deleted: the nominal ratio is subtracted out to calculate delta

david archer 8/21/2018 8:55 AM
Deleted: .

Joel Blum 8/6/2018 12:23 PM
Comment [10]: ok thanks for writing this. It helps me in seeing behind the curtain.

fractionations are calculated by subtracting the expected mass dependent fractionation, to produce a composite quantity Δ value. The solver finds the impact of the fractionation mechanisms on the steady-state isotopic signatures in the Hg system: the expression of the isotope effects within the kinetic ocean Hg cycle.

2.4 The Anthropogenic Perturbation

Human activity has resulted in significantly increased Hg emission to the global biosphere since about 1850 (Streets et al., 2011;Streets et al., 2017;Amos et al., 2013;Horowitz et al., 2014), which has lead to an increase in Hg deposition to the ocean. Because of the tendency for Hg to recycle in the environment, the relationship between emissions and deposition is not simple and immediate, but rather reflects the entire cumulative emission and re-emission of Hg. Guided by a reconstructed history of atmospheric Hg through time (Streets et al., 2017), we subject our model to a 4 times increase in Hg deposition, following an initial spin-up equilibration period of 10,000 years. The beginning of the anthropogenic period corresponds to approximately the year 1850. We show natural steady-state results from model year 1850, which are useful for understanding how the ocean Hg cycle works, and contemporary results from model year 2010, for comparison with field measurements. Anthropogenically enhanced deposition is continued at a constant rate until the year 2100, after which we follow two scenarios: an abrupt and unrealistic return to natural Hg deposition fluxes, useful to determine the time constant of the oceanic recovery, and a "hangover" scenario in which an abrupt cessation of human Hg emissions triggers a gradual slowdown of enhanced deposition, over an ocean overturning time scale of 1,000 years.

2.5 Method Limitations

The steady state assumption in the Hg solvers limits the ability of Hg-HAMOCC to explore detailed shallow-water interactions of turbulence, ventilation, and photochemistry, and the physics of the tracer advection code preclude exploration of processes on short time scales, such as the seasonal cycle near the surface. The model allows us to explore the interaction of the Hg chemistry and particle adsorption with the ocean circulation on long time scales.

A peculiarity of the surface ocean solver is that fluxes of Hg across the sea surface are always locally balanced, by construction, neglecting the impact of any upwelling Hg driving sea surface Hg concentrations and evasion rates to higher values. Similarly to the treatment of O_2 gas in HAMOCC (Maier-Reimer and Bacastow, 1990), the Hg concentrations in the surface box (50 m) are maintained at atmospheric saturation through the iterations in the advection scheme. The concentrations in the box below that (to 125 m) are comprised of 25% saturation while the other 75% is driven by subsurface advection. Because Hg concentrations in the top box are determined by a balance of fluxes with the atmosphere, in places where surface divergence brings up Hg from below, the advective upwelling source is missed by Hg-HAMOCC, which will underestimate the Hg surface concentrations and degassing rates somewhat. To use the model to simulate a transient uptake of Hg by the ocean in response to a change in the surface rain rate, we can track the change in global ocean inventory of Hg with time, but the fluxes determined by the solver at the air-sea interface will balance to zero, locally and at all times, defiant

david archer 8/21/2018 8:55 AM
Deleted:

david archer 8/21/2018 8:55 AM
Deleted: for centuries

david archer 8/21/2018 8:55 AM
Deleted: of

david archer 8/21/2018 8:55 AM
Deleted: Motivated

david archer 8/21/2018 8:55 AM
Deleted: .5

david archer 8/21/2018 8:55 AM
Deleted: spinup

Joel Blum 5/16/2018 9:54 AM
Comment [11]: I see the inflection in lake seds at 1850, which is typically called the tart of the industrial revolution

david archer 8/21/2018 8:55 AM
Deleted: about

david archer 8/21/2018 8:55 AM
Deleted: 1880 in reality

david archer 8/21/2018 8:55 AM
Deleted: the

david archer 8/21/2018 8:55 AM
Deleted: emission

david archer 8/21/2018 8:55 AM
Deleted: for 220 years, corresponding to s... [30]

david archer 8/21/2018 8:55 AM
Deleted: the Hg deposition rate abruptly d... [31]

david archer 8/21/2018 8:55 AM
Deleted: decrease is simpler than the reali... [32]

david archer 8/21/2018 8:55 AM
Deleted: from the ocean itself would fuel ... [33]

david archer 8/21/2018 8:55 AM
Deleted: to the ocean for centuries and lon... [34]

david archer 8/21/2018 8:55 AM
Deleted: . We also simulate

Joel Blum 8/4/2018 3:25 PM
Comment [12]: I changes but to and—pl... [35]

david archer 8/21/2018 8:55 AM
Deleted: , but

david archer 8/21/2018 8:55 AM
Deleted: much

david archer 8/21/2018 8:55 AM
Deleted: that anyway

david archer 8/21/2018 8:55 AM
Deleted: net sea surface fluxes of Hg are a... [36]

of the net fluxes that are filling the deep ocean with Hg. The top box of the model (50 m) serves as a sort of boundary condition for Hg.

david archer 8/21/2018 8:55 AM
Deleted: . This is similar to the treatment of O_2 in HAMOCC, for similar reasons

3 Results

3.1 Particle Sinking versus the Overturning Circulation

david archer 8/21/2018 8:55 AM
Deleted: 3.1 Reaction Kinetics and Path ... [37]

There are two competing mechanisms for Hg invasion into the deep ocean: advection by the overturning circulation and the flux of Hg adsorbed on sinking particles. We use our model to explore the interaction of these pathways. There are two end-member cases to consider; one with particles dominating the distribution and transport of Hg, and the other with circulation dominating. The particle-flux dominating end member condition can be achieved in Hg-HAMOCC by disabling the advection of the Hg tracers (Figure 8, orange line). In the steady state, in order to achieve Hg concentrations that are not changing through time, the vertical flux of Hg through the water column must be the same at all depth levels. The flux of sinking POC decreases with depth in the ocean, because it gets eaten. The abundant POC sinking flux in the surface ocean carries the same Hg sinking flux as the rarefied POC sinking flux in the deep sea.

This means that in the steady state, the POC in the deep sea has to carry more Hg than it would in the surface ocean. The adsorbed Hg is linearly related to the dissolved Hg by the adsorption equation (1). Rearranging (1) gives:

$$[\text{Hg-P}] = [\text{Hg(II)}]\ Kd\ [\text{POC}] \qquad \text{(eqn. 2)}$$

If we take the sinking Hg-P flux to be proportional to [Hg-P] (assuming a uniform sinking velocity), then a decrease in the flux of POC (proportional to [POC] for the same reason), requires a higher dissolved [Hg(II)]. The result is that, in the steady state, Hg concentrations rise with depth in the ocean, to compensate for the decrease in sinking POC flux. A smaller POC sinking flux will have to carry a higher Hg concentration in order to sustain the required depth-uniform Hg flux, and the higher adsorbed Hg concentration requires a higher Hg concentration in the water column.

The other end-member case comes much closer to the observed distribution of Hg in the deep ocean. When circulation dominates, and particle transport of Hg is disabled, the Hg concentrations maintained in the surface ocean (by balancing evasion against deposition) are imposed on the deep ocean, resulting in a nearly uniform distribution of Hg throughout the ocean (Figure 8, blue line). There are some regional variations in Hg in this scenario, but they are not systematic, as compared to the clear Pacific–Atlantic differences exhibited by nutrient-type elements (concentrated in the Pacific) versus by strongly scavenged elements like Al (concentrated in the Atlantic, where deposition is more intense).

The balance between advection versus sinking particles affects the uptake of anthropogenic Hg by the ocean. Profiles of total Hg changes from pre-anthropogenic to present-day, after 130 years of enhanced Hg deposition, are shown in Figure 3. If particles are neglected or sink so slowly as to be negligible in the Hg cycle, there is a sharp surface spike in Hg concentrations in the model simulation of the present-day (2010), due to increased deposition. An increasing importance of particle transport tends to moderate a surface ocean spike, while transferring much of the anthropogenic Hg load to a

david archer 8/21/2018 8:55 AM
Deleted: In the particle-dominating case, the steady state constraint is that the vertical flux of Hg has to be depth-invariant; the fluxes have to balance at any depth level.

david archer 8/21/2018 8:55 AM
Deleted: density

david archer 8/21/2018 8:55 AM
Deleted: density

david archer 8/21/2018 8:55 AM
Formatted: Font color: Auto

david archer 8/21/2018 8:55 AM
Deleted: –

Joel Blum 5/16/2018 10:21 AM
Comment [13]: shouldn't this be 2018-1880 = 138 years?

david archer 8/2/2018 1:43 PM
Comment [14]: I've seen 2010 as present day in Hg modelling, maybe because it sort of represents when the measurements were made. We could do 2018 or whever.

david archer 8/21/2018 8:55 AM
Deleted: 230

david archer 8/21/2018 8:55 AM
Formatted: Font color: Auto

david archer 8/21/2018 8:55 AM
Deleted: 9

Joel Blum 7/31/2018 4:37 PM
Comment [15]: wording needs attention here

david archer 8/21/2018 8:55 AM
Deleted: analog

david archer 8/21/2018 8:55 AM
Deleted:

david archer 8/21/2018 8:55 AM
Deleted: ,

subsurface maximum corresponding to the location of POC degradation in the thermocline. Particulate Hg transport to depth is required in order to simulate a subsurface maximum in Hg concentration, as observed in the present-day real ocean. In the steady state, with no anthropogenic enhanced deposition, a somewhat slower Hg sinking flux would still generate a subsurface maximum, but it is harder to have a subsurface maximum at the end of a period of enhanced Hg deposition, as today.

Figure 9 shows the total ocean inventory of anthropogenic Hg throughout the Anthropogenic deposition period (ending in the year 2100) and beyond, as a function of the Hg particle sinking velocity. Particle transport has only a minor impact on the global rate of Hg uptake during the Anthropocene stage, but strong particle transport has the effect of sequestering the anthropogenic Hg deeper in the ocean (Figure 3), where it is retained somewhat longer than in models with less particle transport. The model, when forced with an instantaneous end to anthropogenic emissions, predicts that the ocean will continue degassing Hg for 1000 years. When this prediction is turned around, to impose a condition that the Hg deposition rate declines over 1000 years after the year 2100, the duration of the anthropogenic Hg load on the oceans increases to several thousand years.

3.2 Model sensitivity to reaction kinetics.

For each of eight kinetic rate constant parameters in the Hg system, we ran simulations to a natural steady state with factor-of-two increases and decreases in each parameter in turn, as shown in Figure 10. In general, increasing the rate constant for a given reaction will increase the concentration of the product, and decrease that of the reactant. The other species' concentrations will also change in the new steady state balance. The concentration of Hg overall depends on the rate of Hg removal from the system, primarily by gas evasion of the minor species Hg(0), with secondary sinks by DMHg evasion and Hg(II) adsorption onto sinking particles (Table 1). Increasing the rate of MMHg production from Hg(II), for example, decreases [Hg(II)] and increases [MMHg]. The concentration of DMHg increases due to its close coupling with MMHg (see Figure 1).

Changes in the rate constants that produce or consume Hg(0) tend to result in larger changes in Hg concentrations than the rate constants for reactions that involve DMHg, because Hg(0) is responsible for a larger fraction of the gas evasion flux. The exception is reductive degradation of MMHg to Hg(0), which occurs primarily in the surface ocean, changing the MMHg concentration there without changing concentrations appreciably in the deep ocean. The highest model sensitivity in the suite of runs is to the rate of evasion of Hg(0), which drive large changes in the total Hg concentration of the entire ocean, in the steady state.

In general, the rates of chemical transformation of Hg are much faster than that of ocean overturning circulation, so the distribution of Hg species at any location reflects a local balance between sources and sinks of each form of Hg. However, reactions at the sea surface that provide a pathway for Hg evasion into the atmosphere have the potential to alter the Hg concentrations throughout the ocean in the steady state.

david archer 8/21/2018 8:55 AM
Deleted: .

Joel Blum 7/31/2018 3:06 PM
Comment [16]: is this what you mean here?

david archer 8/21/2018 8:55 AM
Deleted: 10

david archer 8/21/2018 8:55 AM
Deleted: uptake

david archer 8/21/2018 8:55 AM
Deleted: in that deposition

david archer 8/21/2018 8:55 AM
Deleted: anthropocene

david archer 8/21/2018 8:55 AM
Deleted: 9

david archer 8/21/2018 8:55 AM
Deleted: .

david archer 8/21/2018 8:55 AM
Deleted: our 230-

david archer 8/21/2018 8:55 AM
Deleted: "anthropocene" ending in the present day

david archer 8/21/2018 8:55 AM
Deleted: The top panel in Figure 10 shows the result of a sudden (unrealistic) return to pre-anthropogenic Hg deposition rates, while in the bottom panel the rate of Hg deposition decreases exponentially from anthropogenic values with a time scale of 1000 years (a "hangover" scenario.

3.2 Isotopic Fractionation

Isotopic fractionations in the Hg cycle can be "expressed" in the isotopic signatures of Hg species, or not, depending on how the fractionating process fits into the network of reactions in the cycle. Figure 11 shows the isotopic compositions of Hg species resulting from a variety of fractionation mechanisms, in schematic diagrams of the ocean Hg cycle. Red numbers indicate isotopic fractionations and black numbers show global mean oceanic isotopic compositions. The results represent pre-anthropogenic steady state. The model is run to equilibrium for each of 7 fractionation mechanisms in isolation, and finally for all mechanisms combined. For ease of comparison with oceanic measurements, all scenarios are subject to fractionation in Hg deposition as indicated by the red numbers next to these fluxes. Figure 12 shows depth profiles of isotopic composition. Figure 13 shows maps of isotopic compositions, at the sea surface and at depth.

A guiding principle in understanding these results is that in the steady state the isotopic composition of the sink fluxes have to balance the isotopic compositions of the inputs of Hg(II) from rain and Hg(0) from atmosphere-sea surface exchange. A fractionation mechanism that alters the isotopic signature of one of the sink fluxes will require the steady-state signatures of the other sink fluxes to change in compensation. Then the values of the other species, MMHg, and Hg(II), are pulled in various ways by their connections with the two potential gases.

3.2.1 Gas Evasion Fractionations

The schematic diagram in Figure 11a shows the fractionation associated with evasion of Hg(0) to the atmosphere. The lighter isotope reacts faster (as is typical), leaving a dissolved Hg(0) pool that has residually higher δ^{202}Hg, by about +0.17‰. The Hg(0) evasion flux has a δ^{202}Hg value, from the source isotopic composition of 0.17‰ adjusted for the fractionation of -0.4‰, of -0.23‰, which is lower than the weighted sum of the input fluxes (+0.13‰), and must be balanced by the loss of Hg with a more positive δ^{202}Hg value, by evasion of high δ^{202}Hg DMHg and burial of deep water Hg(II) adsorbed onto particles. The depth dependence of the response is weak (Figure 12a), but variations in particle export from the surface ocean perturb the spatial uniformity of δ^{202}Hg(0) (Figure 13a). Fractionation in DMHg degassing (Figure 11b) is similar in that the δ^{202}Hg of the degassing fractionating species (DMHg) becomes more positive in the residual fraction. Because DMHg is not returned to the Hg pool as quickly in the model as Hg(0), the isotopic deviation in DMHg does not pass to the other pools, which reflect the balance of the source fluxes.

3.2.2 Reaction Fractionations

The expression (or not) of a fractionation in a specific reaction pathway in the Hg cycle depends on the web of reactions between the species and the mass balance constraints. Fractionation during the reduction step from Hg(II) to Hg(0) (Figure 11c and d) pulls the δ^{202}Hg value of Hg(0) to a lower value, requiring a positive excursion in the δ^{202}Hg value of DMHg to compensate. The δ^{202}Hg values of Hg(II) and MMHg follow DMHg to higher values. This fractionation does lead to surface–deep isotopic contrast in δ^{202}Hg, and regional variations at the sea surface and in the deep ocean, reflecting

david archer 8/21/2018 8:55 AM
Deleted: (or not)… in the isotopic signatu ... [38]

david archer 8/21/2018 8:55 AM
Deleted: degassing flux, a combination of Hg(0) and DMHg degassing fluxes, has to balance isotopically the input by Hg(2+) rain, which is 0.4‰ in δ^{202} and 0.05‰ in Δ^{199}. Some fractionation effect that we impose in the model pulls the isotop ... [39]

Joel Blum 7/31/2018 1:50 PM
Comment [17]: use either Hg^{2+} or Hg(II), but not Hg(II)

david archer 8/21/2018 8:55 AM
Deleted: 2+),

david archer 8/21/2018 8:55 AM
Deleted: It has been observed that there is a large difference in the D199 values of MMHg versus Hg(2+) in ocean surface waters (MMHG results from fish: (Blum et al., 2013)). We were forced to modify the web of reactions and kinetics proposed by (Semeniuk and Dastoor, 2017), in particular the formulation of the interreaction between Hg(2+) and MMHg. In (Semeniuk and Dastoor, 2017), MMHg is demethylated to Hg(2+) directly. When configured in this way, the Hg cycle was unable to fractionate MMHg without Hg(2+) following along, because of this reaction. The isotopic composition of total Hg throughout the entire ocean picked up this fractionation signature. A solution is to alter the reaction web so that demethylation produces an intermediary Hg(0), which homogenizes with the rest of the Hg(0) pool before fueling a necessary next step to Hg(2+), which takes place at a faster rate constant than in (Semeniuk and Dastoor, 2017), to compensate for the greater overall traffic of Hg(0) going to Hg(2+). This pathway is consistent with the photochemical mechanism for Hg reaction, which involves accepting an electron to form an intermediary Hg(1). ... [40]

david archer 8/21/2018 8:55 AM
Deleted: Beginning with gas exchange fractionation in …he schematic diagram in F ... [41]

Joel Blum 5/16/2018 11:08 AM
Comment [18]: this sentence needs clarification/reorking

david archer 8/21/2018 8:55 AM
Deleted: an… δ^{202}Hg value, from the sour ... [42]

david archer 8/21/2018 8:55 AM
Deleted: 3

david archer 8/21/2018 8:55 AM
Deleted: Fractionating the reduction step from Hg(2+) to Hg(0) (Figure 11d) has only a slight impact on the isotopic signatures of any of the species, because there is more Hg(0) produced from MMHg than from Hg(2+). In constrast, fractionating the MMHg -> Hg(0) step (Figure 11e) causes MMHg to get lighter, and to pass an ... [43]

differences in particle scavenging in productive areas and the differing fractionation due to photochemistry in the surface ocean. The Δ^{199}Hg isotopic system behaves similarly, with differences due to different isotopic signatures of wet and dry Hg deposition, and with the difference that most of the surface/deep and deep Pacific/Atlantic contrasts in Δ^{199}Hg values can be attributed to this fractionation mechanism alone (Figure 12).

Fractionation in the photochemical MMHg → Hg(0) reaction step (Figure 11e and f) causes an increase in the δ^{202}Hg value of MMHg, which is passed on to DMHg and Hg(II). The Hg(0) evasion flux has only slightly lower δ^{202}Hg than the mean deposition flux, balanced by slightly higher δ^{202}Hg in the DMHg evasion and Hg(II) loss on particles. In contrast to Hg(II) reduction, MMHg reduction does not lead to surface/deep δ^{202}Hg contrast in the Hg(II) (Figures 12 and 13), but it does lead to an enrichment in Δ^{199}Hg of MMHg in the surface ocean (Figure 14), consistent with the measurements of fish Hg by Blum et al (2013), and in contrast with the apparent Δ^{199}Hg of Hg(II) in particles from the upper ocean derived from (Motta LC, submitted).

Fractionation in MMHg production (Figure 11g) results in a decrease in δ^{202}Hg of MMHg, forcing δ^{202}Hg values of Hg(II) to increase in compensation. The higher δ^{202}Hg values of Hg(II) on sinking particles offsets slightly lower δ^{202}Hg values of Hg(0) and DMHg evasion to the atmosphere. Fractionation in biologically mediated MMHg degradation (Figure 11h) acts in the opposite sense for δ^{202}Hg values due to the opposite direction of the reaction. Both fractionation mechanisms lead to horizontal heterogeneity of δ^{202}Hg in the surface ocean, and a contrast between deep Atlantic and Pacific values (Figures 12 and 13). These mechanisms do not impact Δ^{199}Hg values because they are purely mass dependent fractionations. Hg(II) adsorption onto particles generates horizontal gradients in δ^{202}Hg of the surface ocean (Figure 13), but in the global mean the fractionation between the surface ocean and deep ocean is very small (Figure 12).

The Δ^{200}Hg isotopic system does not fractionate internally in the ocean, but rather the ocean acts to integrate the isotopic signature of the surface forcing mechanisms, wet and dry deposition. If the deposition is taken to be spatially uniform, the oceanic distribution of Δ^{200}Hg values will also be uniform throughout the ocean (Figure 15). The global mean Δ^{200}Hg values of the ocean might serve as a constraint on the relative magnitudes of the wet and dry fluxes (Figure 16). Regional variations in Δ^{200}Hg values of the ocean may arise from heterogeneity in the deposition fluxes. In Figure 17, the deposition flux of Hg(II) was doubled in each of the Atlantic, Pacific, and Indian basins in turn and the model run to a natural equilibrium. Variations in the Δ^{200}Hg values of deposition into the surface waters of the basin can also be seen, in a muted way, in the Δ^{200}Hg values at 3 km depth in the ocean. However it must be noted that the predicted variations are small (<0.01‰) and with current analytical methods they would be impossible to measure.

david archer 8/21/2018 8:55 AM

Deleted: Depth profiles of Hg(2+) δ^{202} values are shown in Figure 12. A fractionation in Hg adsorption onto particles tends to leave behind a residually heavy Hg throughout the entire ocean, in response to the isotopically negative Hg burial flux. The surface is held closer than the deep to the 0‰ signature of Hg(2+) atmospheric deposition. The deep ocean Hg is actually isotopically heavier than the surface, counter to the intuition that adsorbing and removing isotopically light Hg from the surface ocean should leave the surface ocean residually heavy. Fractionation in MMHg production leaves Hg(2+) in the deep ocean residually heavy, while fractionation in MMHg reduction results in Hg(2+) that is isotopically light. In both cases, the isotopic composition near the sea surface is again held near 0‰. ... [44]

4 Conclusions

We have embedded a model of Hg chemistry and dynamics into the HAMOCC off-line ocean tracer advection model, including treatment of isotopic fractionation of Hg in the ocean Hg cycle. The efficiency of the model makes it possible to

david archer 8/21/2018 8:55 AM

Deleted: for the first time

do numerous sensitivity experiments for testing hypotheses and developing intuition about this complex system: 55 simulations of over 10 kyr each are presented in this paper.

The model demonstrates that the Hg cycle in the ocean is closer to an advective end member than to a system in which transport on sinking particles dominates. The interplay of advection by fluid flow and sinking of Hg adsorbed on sinking particles is illustrated by end-member cases in which one or the other dominates. In an advection-dominated case in which particle transport is disabled, the Hg concentration in steady state is relatively uniform with depth, displaying the same pattern as for salinity. In a particle-dominated scenario in which fluid advection of Hg is disabled, the concentration of Hg in steady state increases with depth, in proportion to the decrease in the POC sinking flux with depth (due to particle decomposition). This is because in the steady state in which Hg concentrations are not changing with time, the sinking flux of Hg through the ocean must be the same (on a horizontal average) at all depth levels.

A series of sensitivity runs with different Hg-P sinking velocities shows that the observed present-day subsurface maximum in Hg(II) is a product of Hg sinking on particles and the anthropogenic increase in Hg deposition to the surface ocean. Given the 4-times enhanced Hg deposition flux since about 1850 (Streets et al., 2017), if there were no Hg sinking and subsurface release from particles, the highest Hg concentrations would be at the sea surface today. Anthropogenic Hg sinking on particles does not have a strong impact on the net uptake rate of anthropogenic Hg by the ocean, but if the enhanced rates of Hg deposition were suddenly to return to natural levels, a model with strong Hg sinking takes longer to shed its anthropogenic Hg burden. Since oceanic Hg evasion will be recycled and re-deposited, the ocean system seems poised to buffer the environmental Hg concentration for thousands of years.

We show the sensitivity of the steady-state (pre-Anthropogenic, 1850) Hg species concentrations to eight kinetic rate constants in the aqueous Hg cycle. Allowing a reaction to proceed more quickly than a base case tends to result in more of the product and less of the reactant, but the magnitude of the change, and the impact on the rest of the Hg species and the total Hg concentration, vary widely between the various reactions. Changes to the budget of Hg(0), the evasion of which is the dominant loss mechanism for Hg in surface waters, have a strong impact on the rest of the Hg concentrations. Changes to reactions involved in the MMHg budget have a stronger impact on the Hg cycle than changes to DMHg sources or sinks, because MMHg is kinetically tied more closely to Hg(II).

Isotopic variations in Hg have multiple "dimensions" of fractionation, with mass dependent fractionation produced by most processes, and several forms of mass-independent fractionation produced by photochemical reactions. The Hg cycle in the ocean is complex enough that a model is required to predict the "expression" of isotopic fractionations in processes, on the isotopic signatures of Hg species in the ocean, and on the distribution of variations in those signatures. There is wide variation in the expression of isotope fractionation effects in the isotopic composition of Hg standing stocks. In the model, surface/deep contrasts in δ^{202}Hg (and Δ^{199}Hg) are due largely to fractionation in the rate of Hg(II) biological+photochemical reduction. This mechanism also generates a contrast between Atlantic and Pacific deep isotopic compositions. The photochemical reduction of MMHg generates a dramatic contrast between the Δ^{199}Hg of MMHg and Hg(II) in the surface ocean, consistent with isotopic measurements of fish (Blum et al., 2013). Multiple mechanisms produced patterns in sea

david archer 8/21/2018 8:55 AM
Deleted: , which is useful

david archer 8/21/2018 8:55 AM
Deleted: a purely…n advective end memb ... [45]

david archer 8/21/2018 8:55 AM
Deleted: […g(2+)]…I) is a product of Hg ... [46]

david archer 8/21/2018 8:55 AM
Deleted: can be used to constrain Hg cycling, especially powerfully because of the…ave n ... [47]

surface δ^{202}Hg signatures, some creating high δ^{202}Hg excursions in productive areas and some producing low δ^{202}Hg excursions (these mechanisms are, for high δ^{202}Hg excursions in e.g. the equatorial Pacific: MMHg photoreduction, biological MMHg production, and Hg(II) adsorption, and for low δ^{202}Hg excursions: Hg(0) evasion, Hg(II) reduction, biological MMHg production, MMHg biodegradation, and Hg(II) adsorption). The Δ^{199}Hg system in the model is entirely driven by photochemical reactions (Hg(II) and MMHg photo reduction). In reality there may be variations in source input, but the rates and isotopic signatures of Hg deposition are spatially uniform in the model. Both photochemical mechanisms produce heterogeneity at the sea surface driven by differences in particle export. The only depth contrast in Δ^{199}Hg predicted by the model is for Δ^{199}Hg of MMHg due to MMHg photo-reduction. The Δ^{200}Hg of the ocean on global average in the model reflects the balance of wet vs. dry deposition of Hg (Hg(II) vs. Hg(0)), and regional variations in those rain rates at the sea surface in the model may be weakly represented in the isotopic composition of the deep ocean basins.

References

Amos, H. M., Jacob, D. J., Streets, D. G., and Sunderland, E. M.: Legacy impacts of all-time anthropogenic emissions on the global mercury cycle, Global Biogeochemical Cycles, 27, 410-421, 10.1002/gbc.20040, 2013.

Anderson, R. F., Cheng, H., Edwards, R. L., Fleisher, M. Q., Hayes, C. T., Huang, K. F., Kadko, D., Lam, P. J., Landing, W. M., Lao, Y., Lu, Y., Measures, C. I., Moran, S. B., Morton, P. L., Ohnemus, D. C., Robinson, L. F., and Shelley, R. U.: How well can we quantify dust deposition to the ocean?, Philosophical Transactions of the Royal Society a-Mathematical Physical and Engineering Sciences, 374, 10.1098/rsta.2015.0285, 2016.

Archer, D. E., Eby, M., Brovkin, V., Ridgewell, A. J., Cao, L., Mikolajewicz, U., Caldeira, K., Matsueda, H., Munhoven, G., Montenegro, A., and Tokos, K.: Atmospheric lifetime of fossil fuel carbon dioxide, Ann. Reviews Earth Planet Sci., 37, 117-134, 2009.

Balogh, S. J., Tsui, M. T. K., Blum, J. D., Matsuyama, A., Woerndle, G. E., Yano, S., and Tada, A.: Tracking the Fate of Mercury in the Fish and Bottom Sediments of Minamata Bay, Japan, Using Stable Mercury Isotopes, Environmental Science & Technology, 49, 5399-5406, 10.1021/acs.est.5b00631, 2015.

Bergquist, B. A., and Blum, J. D.: Mass-dependent and -independent fractionation of Hg isotopes by photoreduction in aquatic systems, Science, 318, 417-420, 10.1126/science.1148050, 2007.

Bergquist, B. A., and Blum, J. D.: The Odds and Evens of Mercury Isotopes: Applications of Mass-Dependent and Mass-Independent Isotope Fractionation, Elements, 5, 353-357, 10.2113/gselements.5.6.353, 2009.

Biswas, A., Blum, J. D., and Keeler, G. J.: Mercury storage in surface soils in a central Washington forest and estimated release during the 2001 Rex Creek Fire, Science of the Total Environment, 404, 129-138, 10.1016/j.scitotenv.2008.05.043, 2008.

Blum, J. D.: Mesmerized by mercury, Nature Chemistry, 5, 1066-1066, 10.1038/nchem.1803, 2013.

Blum, J. D., Popp, B. N., Drazen, J. C., Choy, C. A., and Johnson, M. W.: Methylmercury production below the mixed layer in the North Pacific Ocean, Nature Geoscience, 6, 879-884, 10.1038/ngeo1918, 2013.

Blum, J. D., Sherman, L. S., and Johnson, M. W.: Mercury Isotopes in Earth and Environmental Sciences, in: Annual Review of Earth and Planetary Sciences, Vol 42, edited by: Jeanloz, R., Annual Review of Earth and Planetary Sciences, 249-269, 2014.

Bowman, K. L., Hammerschmidt, C. R., Lamborg, C. H., and Swarr, G.: Mercury in the North Atlantic Ocean: The US GEOTRACES zonal and meridional sections, Deep-Sea Research Part Ii-Topical Studies in Oceanography, 116, 251-261, 10.1016/j.dsr2.2014.07.004, 2015.

Broecker, W. S., and Peng, T.-H.: Gas exchange rate between sea and air, Tellus, 26, 21-35, 1974.

Buchachenko, A. L.: Magnetic isotope effect: Nuclear spin control of chemical reactions, Journal of Physical Chemistry A, 105, 9995-10011, 10.1021/jp011261d, 2001.

Chakraborty, P., Mason, R. P., Jayachandran, S., Vudamala, K., Armoury, K., Sarkar, A., Chakraborty, S., Bardhan, P., and Naik, R.: Effects of bottom water oxygen concentrations on mercury distribution and speciation in sediments below the oxygen minimum zone of the Arabian Sea, Marine Chemistry, 186, 24-32, 10.1016/j.marchem.2016.07.005, 2016.

Chandan, P., Ghosh, S., and Bergquist, B. A.: Mercury Isotope Fractionation during Aqueous Photoreduction of Monomethylmercury in the Presence of Dissolved Organic Matter, Environmental Science & Technology, 49, 259-267, 10.1021/es5034553, 2015.

Joel Blum 8/4/2018 4:28 PM
Comment [19]: this is a difficult sentence to follow. Can you break it into multiple sentences?

david archer 8/21/2018 8:55 AM
Deleted: δ^{202}Hg(2+) include a correlation with the rate of primary productivity in the surface ocean for some mechanisms, but that much of this correlation cancels out in the sum of all processes, because the signs of the impact differ among the processes. Another spatial signature to look for is the gradient in the δ^{202}Hg(2+) of the deep Atlantic vs. Pacific, which results in the model mostly from dark reactions creating and destroying MMHg.

david archer 8/21/2018 8:55 AM
Deleted:

david archer 8/21/2018 8:55 AM
Deleted: Amos, H. M., Jacob, D. J., Streets, D. G., and Sunderland, E. M.: Legacy impacts of all-time anthropogenic emissions on the global mercury cycle, Global Biogeochemical Cycles, 27, 410-421, 10.1002/gbc.20040, 2013. ... [48]

Chen, C. Y., Driscoll, C. T., Lambert, K. F., Mason, R. P., and Sunderland, E. M.: Connecting mercury science to policy: from sources to seafood, Reviews on Environmental Health, 31, 17-20, 10.1515/reveh-2015-0044, 2016.
Clarkson, T. W., and Magos, L.: The toxicology of mercury and its chemical compounds, Critical Reviews in Toxicology, 36, 609-662, 10.1080/10408440600845619, 2006.
Demers, J. D., Sherman, L. S., Blum, J. D., Marsik, F. J., and Dvonch, J. T.: Coupling atmospheric mercury isotope ratios and meteorology to identify sources of mercury impacting a coastal urban-industrial region near Pensacola, Florida, USA, Global Biogeochemical Cycles, 29, 1689-1705, 10.1002/2015gb005146, 2015.
Donovan, P. M., Blum, J. D., Yee, D., Gehrke, G. E., and Singer, M. B.: An isotopic record of mercury in San Francisco Bay sediment, Chemical Geology, 349, 87-98, 10.1016/j.chemgeo.2013.04.017, 2013.
Donovan, P. M., Blum, J. D., Demers, J. D., Gu, B. H., Brooks, S. C., and Peryam, J.: Identification of Multiple Mercury Sources to Stream Sediments near Oak Ridge, TN, USA, Environmental Science & Technology, 48, 3666-3674, 10.1021/es4046549, 2014.
Driscoll, C. T., Mason, R. P., Chan, H. M., Jacob, D. J., and Pirrone, N.: Mercury as a Global Pollutant: Sources, Pathways, and Effects, Environmental Science & Technology, 47, 4967-4983, 10.1021/es305071v, 2013.
Fitzgerald, W. F., Lamborg, C. H., and Hammerschmidt, C. R.: Marine biogeochemical cycling of mercury, Chemical Reviews, 107, 641-662, 10.1021/cr050353m, 2007.
Foucher D, H. H., Al TA, MacQuarrie KT. : Mercury isotope fractionation in waters and sediments of the Murray Brook mine watershed (New Brunswick, Canada): tracing mercury contamination and transformation, Chem. Geol. , 336, 87-95, 2013.
Gebbie, G., and Huybers, P.: The Mean Age of Ocean Waters Inferred from Radiocarbon Observations: Sensitivity to Surface Sources and Accounting for Mixing Histories, Journal of Physical Oceanography, 42, 291-305, 10.1175/jpo-d-11-043.1, 2012.
Gehrke, G. E., Blum, J. D., Slotton, D. G., and Greenfield, B. K.: Mercury Isotopes Link Mercury in San Francisco Bay Forage Fish to Surface Sediments, Environmental Science & Technology, 45, 1264-1270, 10.1021/es103053y, 2011.
Han, S. H., Gill, G. A., Lehman, R. D., and Choe, K. Y.: Complexation of mercury by dissolved organic matter in surface waters of Galveston Bay, Texas, Marine Chemistry, 98, 156-166, 10.1016/j.marchem.2005.07.004, 2006.
Hollweg, T. A., Gilmour, C. C., and Mason, R. P.: Mercury and methylmercury cycling in sediments of the mid-Atlantic continental shelf and slope, Limnology and Oceanography, 55, 2703-2722, 10.4319/lo.2010.55.6.2703, 2010.
Horowitz, H. M., Jacob, D. J., Amos, H. M., Streets, D. G., and Sunderland, E. M.: Historical Mercury Releases from Commercial Products: Global Environmental Implications, Environmental Science & Technology, 48, 10242-10250, 10.1021/es501337j, 2014.
Jiskra M, W. J., Bourdon B, Kretzschmar R. : Solution speciation controls mercury isotope fractionation of Hg(II) sorption to goethite. , Environ. Sci. Technol. , 46, 6654–6662, 2012.
Jonsson, S., Mazrui, N. M., and Mason, R. P.: Dimethylmercury Formation Mediated by Inorganic and Organic Reduced Sulfur Surfaces, Scientific Reports, 6, 10.1038/srep27958, 2016.
Krabbenhoft, D. P., and Sunderland, E. M.: Global Change and Mercury, Science, 341, 1457-1458, 10.1126/science.1242838, 2013.
Kritee, K., Blum, J. D., Johnson, M. W., Bergquist, B. A., and Barkay, T.: Mercury stable isotope fractionation during reduction of Hg(II) to Hg(0) by mercury resistant microorganisms, Environmental Science & Technology, 41, 1889-1895, 10.1021/es062019t, 2007.
Kwon, S. Y., Blum, J. D., Chirby, M. A., and Chesney, E. J.: Application of mercury isotopes for tracing trophic transfer and internal distribution of mercury in marine fish feeding experiments, Environmental Toxicology and Chemistry, 32, 2322-2330, 10.1002/etc.2313, 2013.
Kwon, S. Y., Blum, J. D., Chen, C. Y., Meattey, D. E., and Mason, R. P.: Mercury Isotope Study of Sources and Exposure Pathways of Methylmercury in Estuarine Food Webs in the Northeastern US, Environmental Science & Technology, 48, 10089-10097, 10.1021/es5020554, 2014.
Lamborg, C., Bowman, K., Hammerschmidt, C., Gilmour, C., Munson, K., Selin, N., and Tseng, C. M.: MERCURY in the Anthropocene Ocean, Oceanography, 27, 76-87, 10.5670/oceanog.2014.11, 2014.
Lamborg, C. H., Hammerschmidt, C. R., and Bowman, K. L.: An examination of the role of particles in oceanic mercury cycling, Philosophical Transactions of the Royal Society a-Mathematical Physical and Engineering Sciences, 374, 10.1098/rsta.2015.0297, 2016.
Lehnherr, I., St Louis, V. L., Hintelmann, H., and Kirk, J. L.: Methylation of inorganic mercury in polar marine waters, Nature Geoscience, 4, 298-302, 10.1038/ngeo1134, 2011.
Lehnherr, I.: Methylmercury biogeochemistry: a review with special reference to Arctic aquatic ecosystems, Environmental Reviews, 22, 229-243, 10.1139/er-2013-0059, 2014.
Li, M. L., Sherman, L. S., Blum, J. D., Grandjean, P., Mikkelsen, B., Weihe, P., Sunderland, E. M., and Shine, J. P.: Assessing Sources of Human Methylmercury Exposure Using Stable Mercury Isotopes, Environmental Science & Technology, 48, 8800-8806, 10.1021/es500340r, 2014.
Maier-Reimer, E.: Towards a global ocean carbon model, Prog. Biometeorology, 3, 295-310, 1984.
Maier-Reimer, E., and Hasselmann, K.: Transport and storage of CO2 in the ocean - an inorganic ocean-circulation carbon cycle model, Climate Dynamics, 2, 63-90, 10.1007/bf01054491, 1987.
Maier-Reimer, E., and Bacastow, R.: Modelling of geochemical tracers in the ocean, in: Climate-Ocean Interaction, edited by: Schlesinger, M. E., Kluwer, Netherlands, 233-267, 1990.

Maierreimer, E., Mikolajewicz, U., and Hasselmann, K.: MEAN CIRCULATION OF THE HAMBURG LSG OGCM AND ITS SENSITIVITY TO THE THERMOHALINE SURFACE FORCING, Journal of Physical Oceanography, 23, 731-757, 10.1175/1520-0485(1993)023<0731:mcothl>2.0.co;2, 1993.
Mason, R. P., Choi, A. L., Fitzgerald, W. F., Hammerschmidt, C. R., Lamborg, C. H., Soerensen, A. L., and Sunderland, E. M.: Mercury biogeochemical cycling in the ocean and policy implications, Environmental Research, 119, 101-117, 10.1016/j.envres.2012.03.013, 2012.
Motta LC, B. J., Johnson MW, Washburn SJ, Popp BN, Close H, Umhau B, Benitez-Nelson C, and Hannides C. : Hg cycling in the North Pacific Subtropical Gyre as revealed by Hg isotopes., submitted.
Munson, K. M., Lamborg, C. H., Swarr, G. J., and Saito, M. A.: Mercury species concentrations and fluxes in the Central Tropical Pacific Ocean, Global Biogeochemical Cycles, 29, 656-676, 10.1002/2015gb005120, 2015.
Obrist, D., Agnan, Y., Jiskra, M., Olson, C. L., Colegrove, D. P., Hueber, J., Moore, C. W., Sonke, J. E., and Helmig, D.: Tundra uptake of atmospheric elemental mercury drives Arctic mercury pollution, Nature, 547, 201-+, 10.1038/nature22997, 2017.
Obrist, D., Kirk, J. L., Zhang, L., Sunderland, E. M., Jiskra, M., and Selin, N. E.: A review of global environmental mercury processes in response to human and natural perturbations: Changes of emissions, climate, and land use, Ambio, 47, 116-140, 10.1007/s13280-017-1004-9, 2018.
Ortiz, V. L., Mason, R. P., and Ward, J. E.: An examination of the factors influencing mercury and methylmercury particulate distributions, methylation and demethylation rates in laboratory-generated marine snow, Marine Chemistry, 177, 753-762, 10.1016/j.marchem.2015.07.006, 2015.
Ray, E. A., Moore, F. L., Elkins, J. W., Rosenlof, K. H., Laube, J. C., Rockmann, T., Marsh, D. R., and Andrews, A. E.: Quantification of the SF6 lifetime based on mesospheric loss measured in the stratospheric polar vortex, Journal of Geophysical Research-Atmospheres, 122, 4626-4638, 10.1002/2016jd026198, 2017.
Rodriguez-Gonzalez, P., Epov, V. N., Bridou, R., Tessier, E., Guyoneaud, R., Monperrus, M., and Amouroux, D.: Species-Specific Stable Isotope Fractionation of Mercury during Hg(II) Methylation by an Anaerobic Bacteria (Desulfobulbus propionicus) under Dark Conditions, Environmental Science & Technology, 43, 9183-9188, 10.1021/es902206j, 2009.
Rose, C. H., Ghosh, S., Blum, J. D., and Bergquist, B. A.: Effects of ultraviolet radiation on mercury isotope fractionation during photo-reduction for inorganic and organic mercury species, Chemical Geology, 405, 102-111, 10.1016/j.chemgeo.2015.02.025, 2015.
Schartup, A. T., Mason, R. P., Balcom, P. H., Hollweg, T. A., and Chen, C. Y.: Methylmercury Production in Estuarine Sediments: Role of Organic Matter, Environmental Science & Technology, 47, 695-700, 10.1021/es302566w, 2013.
Schartup, A. T., Ndu, U., Balcom, P. H., Mason, R. P., and Sunderland, E. M.: Contrasting Effects of Marine and Terrestrially Derived Dissolved Organic Matter on Mercury Speciation and Bioavailability in Seawater, Environmental Science & Technology, 49, 5965-5972, 10.1021/es506274x, 2015.
Schartup, A. T., Qureshi, A., Dassuncao, C., Thackray, C. P., Harding, G., and Sunderland, E. M.: A Model for Methylmercury Uptake and Trophic Transfer by Marine Plankton, Environmental Science & Technology, 52, 654-662, 10.1021/acs.est.7b03821, 2018.
Schauble, E. A.: Role of nuclear volume in driving equilibrium stable isotope fractionation of mercury, thallium, and other very heavy elements, Geochimica Et Cosmochimica Acta, 71, 2170-2189, 10.1016/j.gca.2007.02.004, 2007.
Schuster, P. F., Schaefer, K. M., Aiken, G. R., Antweiler, R. C., Dewild, J. F., Gryziec, J. D., Gusmeroli, A., Hugelius, G., Jafarov, E., Krabbenhoft, D. P., Liu, L., Herman-Mercer, N., Mu, C., Roth, D. A., Schaefer, T., Striegl, R. G., Wickland, K. P., and Zhang, T.: Permafrost Stores a Globally Significant Amount of Mercury, Geophysical Research Letters, 45, 10.1002/2017GL075571, 2018.
Semeniuk, K., and Dastoor, A.: Development of a global ocean mercury model with a methylation cycle: Outstanding issues, Global Biogeochemical Cycles, 31, 400-433, 10.1002/2016gb005452, 2017.
Sherman, L. S., Blum, J. D., Franzblau, A., and Basu, N.: New Insight into Biomarkers of Human Mercury Exposure Using Naturally Occurring Mercury Stable Isotopes, Environmental Science & Technology, 47, 3403-3409, 10.1021/es305250z, 2013.
Sherman, L. S., Blum, J. D., Basu, N., Rajaee, M., Evers, D. C., Buck, D. G., Petrlik, J., and DiGangi, J.: Assessment of mercury exposure among small-scale gold miners using mercury stable isotopes, Environmental Research, 137, 226-234, 10.1016/j.envres.2014.12.021, 2015.
Smith-Downey, N. V., Sunderland, E. M., and Jacob, D. J.: Anthropogenic impacts on global storage and emissions of mercury from terrestrial soils: Insights from a new global model, Journal of Geophysical Research-Biogeosciences, 115, 10.1029/2009jg001124, 2010.
Soerensen, A. L., Sunderland, E. M., Holmes, C. D., Jacob, D. J., Yantosca, R. M., Skov, H., Christensen, J. H., Strode, S. A., and Mason, R. P.: An Improved Global Model for Air-Sea Exchange of Mercury: High Concentrations over the North Atlantic, Environmental Science & Technology, 44, 8574-8580, 10.1021/es102032g, 2010.
Sonke JE, S. J., Chmeleff J, Audry S, Blanc G, Dupre B. : Sedimentary mercury stable isotope records of atmospheric and riverine pollution from two major European heavy metal refineries, Chem. Geol. , 279, 90-100, 2010.
Streets, D. G., Devane, M. K., Lu, Z. F., Bond, T. C., Sunderland, E. M., and Jacob, D. J.: All-Time Releases of Mercury to the Atmosphere from Human Activities, Environmental Science & Technology, 45, 10485-10491, 10.1021/es202765m, 2011.
Streets, D. G., Horowitz, H. M., Jacob, D., Lu, Z. F., Levin, L., ter Schure, A. F. H., and Sunderland, E. M.: Total Mercury Released to the Environment by Human Activities, Environmental Science & Technology, 51, 5969-5977, 10.1021/acs.est.7b00451, 2017.

Strok, M., Baya, P. A., and Hintelmann, H.: The mercury isotope composition of Arctic coastal seawater, Comptes Rendus Geoscience, 347, 368-376, 10.1016/j.crte.2015.04.001, 2015.
Sun, R. Y., Streets, D. G., Horowitz, H. M., Amos, H. M., Liu, G. J., Perrot, V., Toutain, J. P., Hintelmann, H., Sunderland, E. M., and Sonke, J. E.: Historical (1850-2010) mercury stable isotope inventory from anthropogenic sources to the atmosphere, Elementa-Science of the Anthropocene, 4, 1-15, 10.12952/journal.elementa.000091, 2016.
Tsui, M. T. K., Blum, J. D., Finlay, J. C., Balogh, S. J., Nollet, Y. H., Palen, W. J., and Power, M. E.: Variation in Terrestrial and Aquatic Sources of Methylmercury in Stream Predators as Revealed by Stable Mercury Isotopes, Environmental Science & Technology, 48, 10128-10135, 10.1021/es500517s, 2014.
Wiederhold, J. G., Cramer, C. J., Daniel, K., Infante, I., Bourdon, B., and Kretzschmar, R.: Equilibrium Mercury Isotope Fractionation between Dissolved Hg(II) Species and Thiol-Bound Hg, Environmental Science & Technology, 44, 4191-4197, 10.1021/es100205t, 2010.
Yang, L., and Sturgeon, R.: Isotopic fractionation of mercury induced by reduction and ethylation, Analytical and Bioanalytical Chemistry, 393, 377-385, 10.1007/s00216-008-2348-6, 2009.
Yin R, F. X., Wang J, Bao Z, Yu B, Chen J. : Mercury isotope variations between bioavailable mercury fractions and total mercury in mercury contaminated soil in Wanshan mercury mine, SW China, Chem Geol., 336, 2013.
Zhang, Y. X., Jaegle, L., and Thompson, L.: Natural biogeochemical cycle of mercury in a global three-dimensional ocean tracer model, Global Biogeochemical Cycles, 28, 553-570, 10.1002/2014gb004814, 2014a.
Zhang, Y. X., Jaegle, L., Thompson, L., and Streets, D. G.: Six centuries of changing oceanic mercury, Global Biogeochemical Cycles, 28, 1251-1261, 10.1002/2014gb004939, 2014b.
Zheng, W., and Hintelmann, H.: Nuclear Field Shift Effect in Isotope Fractionation of Mercury during Abiotic Reduction in the Absence of Light, Journal of Physical Chemistry A, 114, 4238-4245, 10.1021/jp910353y, 2010.
Zheng, W., Obrist, D., Weis, D., and Bergquist, B. A.: Mercury isotope compositions across North American forests, Global Biogeochemical Cycles, 30, 1475-1492, 10.1002/2015gb005323, 2016.

Table 1. Fluxes in Mmol/yr from model kinetic rate constant sensitivity experiments.

Experiment	Hg(0) Evasion	DMHg Evasion	HgP surf	HgP seafloor
Base	3.69	0.07	1.12	0.57
Hg(II) -> MM 2x	3.77	0.08	1.03	0.47
0.5x	3.65	0.06	1.17	0.64
MMHg -> Hg(II) 2x	3.67	0.06	1.14	0.63
0.5x	3.71	0.07	1.10	0.49
Hg(II) -> Hg(0) 2x	3.75	0.06	1.06	0.43
0.5x	3.66	0.07	1.15	0.66
Hg(0) -> Hg(II) 2x	3.68	0.07	1.13	0.66
0.5x	3.70	0.07	1.11	0.46
MMHg -> Hg(0) 2x	3.72	0.06	1.10	0.56
0.5x	3.66	0.08	1.14	0.59
Hg(II) -> DMHg 2x	3.66	0.12	1.10	0.53
0.5x	3.71	0.04	1.12	0.62
MMHg -> DMHg 2x	3.70	0.07	1.12	0.62
0.5x	3.69	0.07	1.12	0.50
DMHg -> MMHg 2x	3.68	0.08	1.11	0.53
0.5x	3.70	0.06	1.12	0.60
Hg(0) Evasion 2x	4.14	0.04	0.70	0.40
0.5x	2.96	0.10	1.81	1.06
DMHg Evasion 2x	3.65	0.06	1.17	0.67
0.5x	3.65	0.06	1.17	0.67

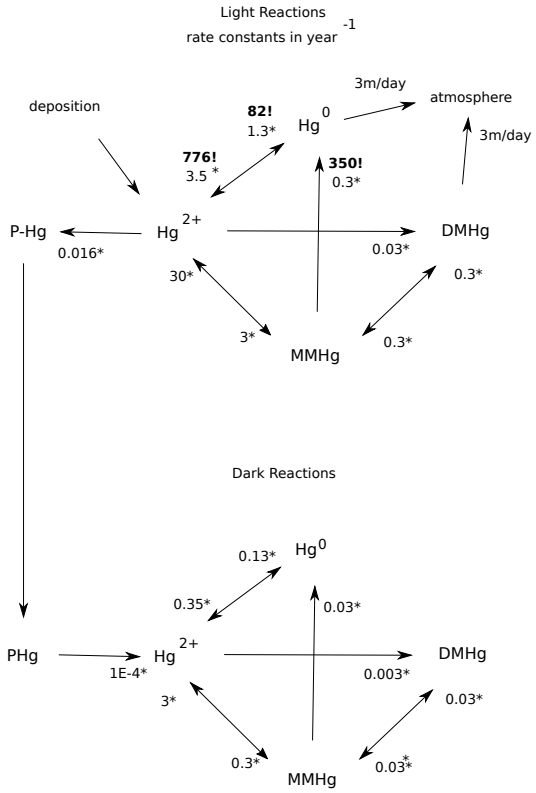

Figure 1. Schematic of the reaction web for Hg speciation in the model. Starred numbers by the arrows show typical values for biologically mediated rate constants, in units of yr^{-1}. Photochemical rate constants are denoted by bold text and exclamation marks (!). Gas evasion rate constants are based on an ocean-average piston velocity of 3 m/day (Broecker and Peng, 1974). Biological rate constants are fit to (Semeniuk and Dastoor, 2017) and (Zhang et al., 2014a), based on first-order degradation kinetics for POC, resulting in a scaling $k_{bio} = 10^{-6}$ [POC](mol/L). Photochemical MMHg degradation rate constant is from (Bergquist and Blum, 2007). Hg(II) photoreduction and Hg(0) photooxidation rate constants are fits to the global budget from (Soerensen et al., 2010).

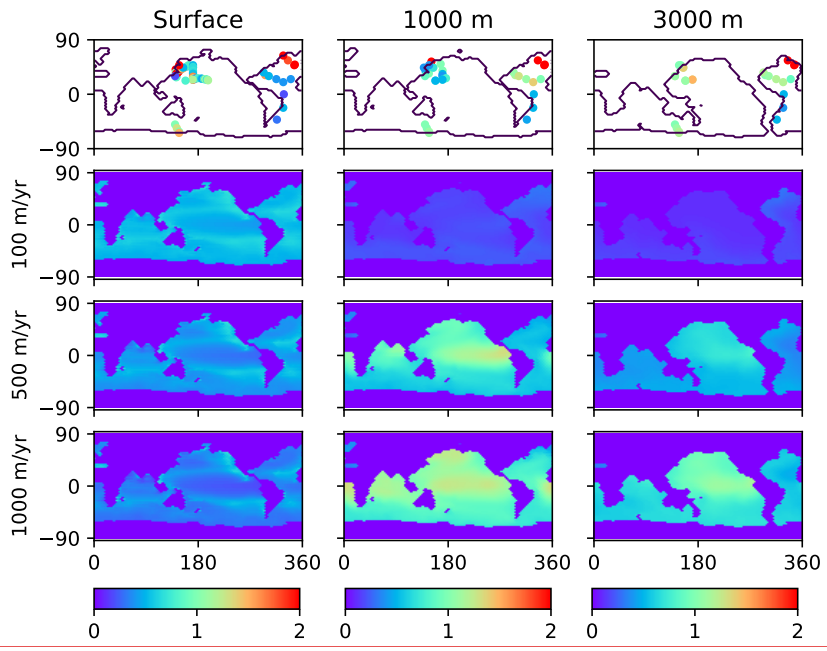

Figure 2. Comparison of Hg(tot) concentrations in pM from the model with data in the top row, from {Laurier, 2004 #6663} and {Zhang, 2014 #6675}, at approximately the depths in the ocean given at the top. Lower three rows are present-day (year 2010) model results using different values of the particulate-bound Hg sinking velocity as indicated by the labels on the left, with 500 m/yr as the the base case.

Joel Blum 7/30/2018 4:29 PM

Comment [20]: I don't get the units or axis labels. label m/yr as sinking velocity, label the panels that contain data as such, give units of Hg concentration etc

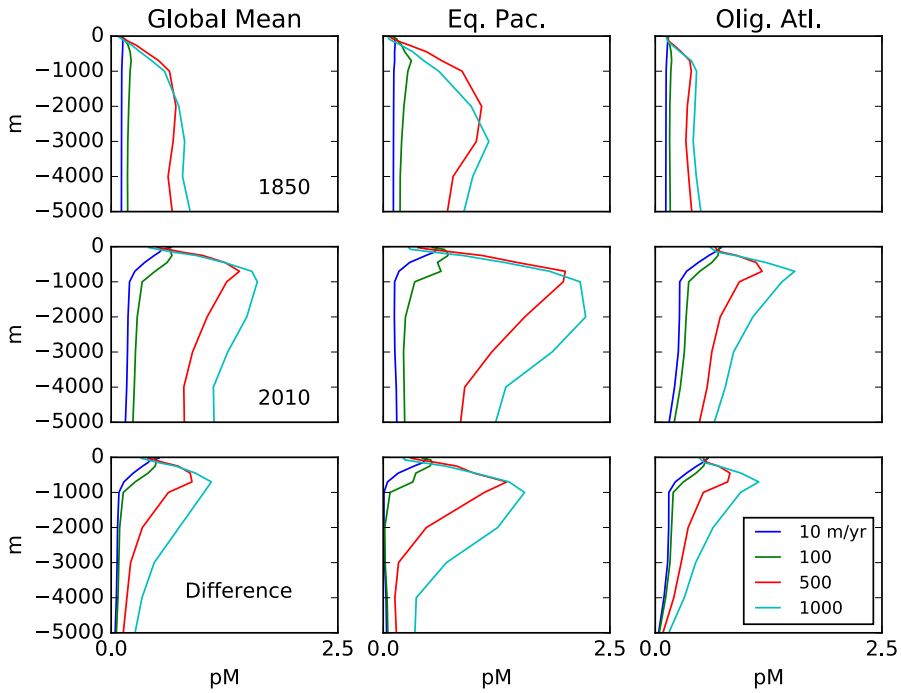

Figure 3. Depth profiles (in meters) of the total Hg concentration in the model, global mean and from locations shown on Figure 4, preanthropogenic (1850), present-day (2010), and the difference between the two, for different values of the particulate-bound Hg flux in m/yr (the base case is 500 m/yr).

Joel Blum 7/31/2018 2:17 PM
Comment [21]: not right

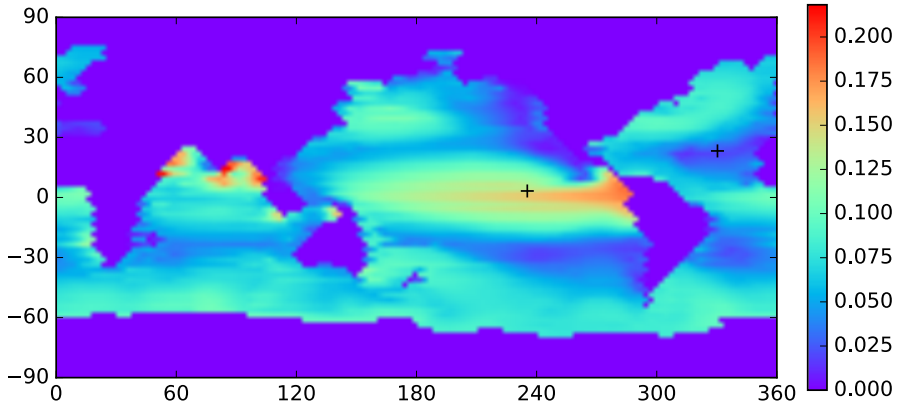

Figure 4. A map of the bound fraction of Hg(II) (relative to bound + unbound), at the sea surface, when the K_d value is $2 \cdot 10^6$. Higher POC concentrations in productive regions lead to higher bound fractions of the Hg(II). Plusses indicate the locations of profiles in Figures 3, 8, 12, 14, and 15.

Joel Blum 8/4/2018 11:45 AM
Comment [22]: If its not too much trouble it would be great to axis labels directly on the figure.

david archer 8/21/2018 8:55 AM
Moved (insertion) [3]

david archer 8/21/2018 8:55 AM
Deleted: 2+)

david archer 8/21/2018 8:55 AM
Deleted: $1 \cdot 10^4$, resulting in approximately 5% bound Hg(2+) in surface waters on average, with higher values in high-POC

david archer 8/21/2018 8:55 AM
Deleted: .

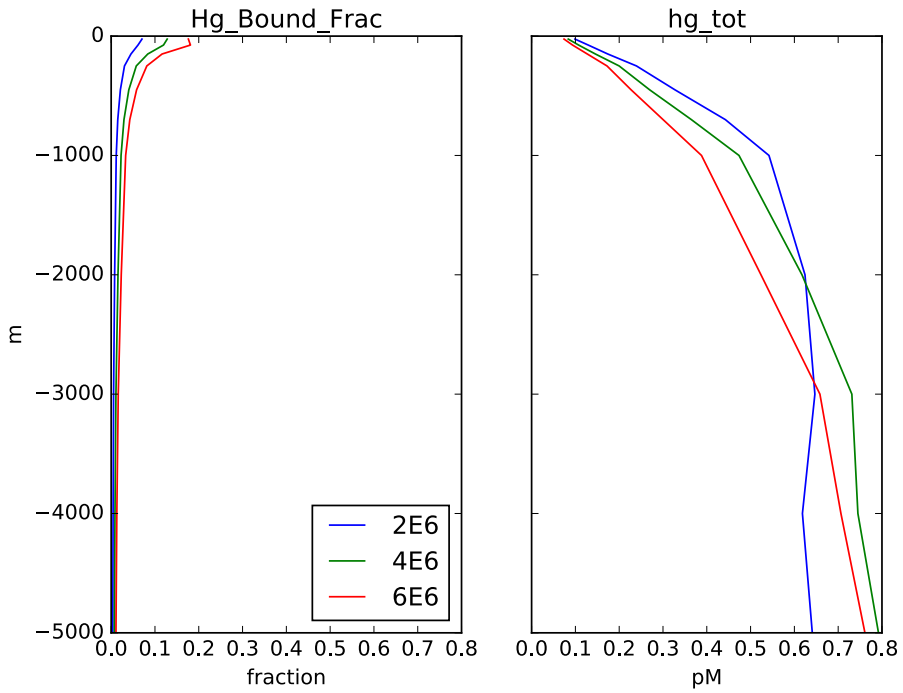

Figure 5. Depth profiles (in meters) of the bound fraction of Hg(II) from the same locations as in Figure 3, as a function of the K_d value, preanthropogenic steady state (1850). A value of $2 \cdot 10^6$ l/kg POC (blue lines) is used in the rest of the model simulations.

david archer 8/21/2018 8:55 AM

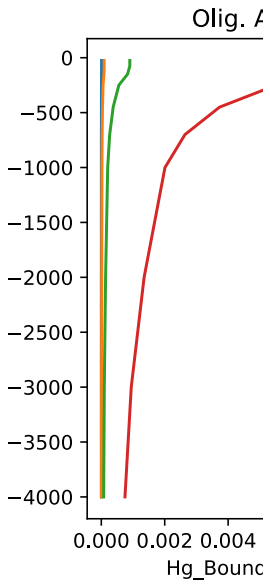

Deleted:

david archer 8/21/2018 8:55 AM

Moved (insertion) [4]

david archer 8/21/2018 8:55 AM

Moved up [3]: Figure 4.

david archer 8/21/2018 8:55 AM

Deleted: 2+)

david archer 8/21/2018 8:55 AM

Deleted: 2

david archer 8/21/2018 8:55 AM

Deleted: .

david archer 8/21/2018 8:55 AM

Deleted: $1 \cdot 10^4$ (red

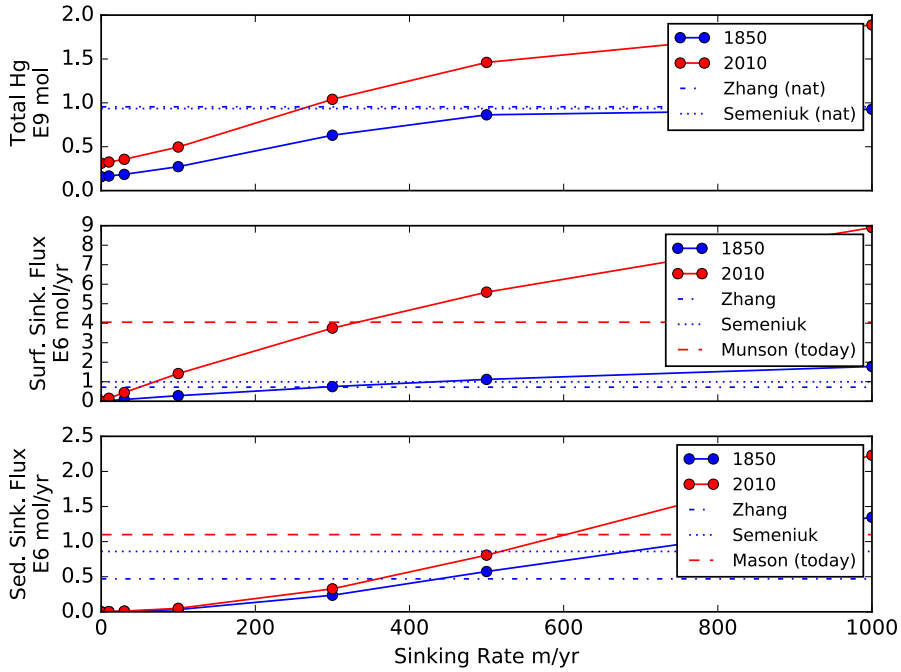

Figure 6. Global model fluxes as a function of Hg(II) sinking velocity imposed in the model. Colors represent preanthropogenic and present-day results from our model. For comparison broken lines are model results from (Zhang et al., 2014a) and (Semeniuk and Dastoor, 2017), sediment trap data from (Munson et al., 2015), 17° N latitude in the Pacific and 60 m water depth, extrapolated globally, and a summary of present-day fluxes from (Mason et al., 2012). A default value of 500 m / year is the base case for the rest of the simulations in this paper.

david archer 8/21/2018 8:55 AM

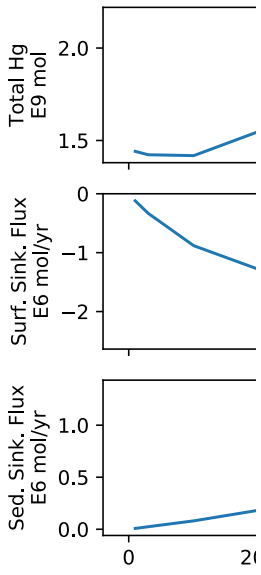

Deleted:

david archer 8/21/2018 8:55 AM

Moved (insertion) [5]

david archer 8/21/2018 8:55 AM

Moved up [4]: Figure 5.

david archer 8/21/2018 8:55 AM

Deleted: Model fluxes as a function of Hg(2+) sinking velocity imposed in the model. A default value of 400 m / year is used in the rest of the simulations. ... [49]

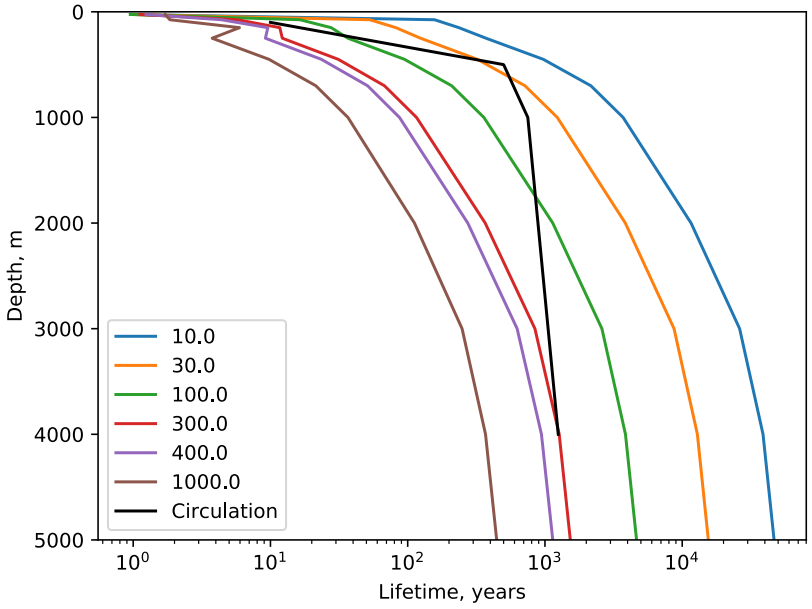

Figure 7. Profiles of the turnover time of Hg(II) with respect to transiting through the system on sinking particles, as a function of the sinking velocity in the legend, in m/yr. The black line is the water age since exposure to the atmosphere derived from the ^{14}C distribution (Gebbie and Huybers, 2012).

david archer 8/21/2018 8:55 AM
Moved up [5]: Figure 6.

david archer 8/21/2018 8:55 AM
Deleted: 2+)

david archer 8/21/2018 8:55 AM
Deleted:

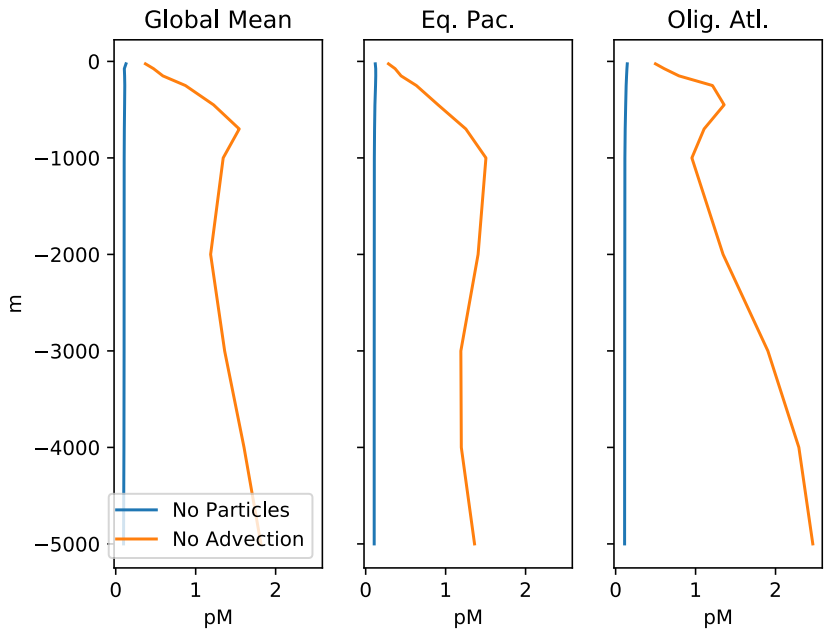

Figure 8. Profiles of mean Hg concentration in (preanthropogenic) steady state, as a function of depth in the ocean, in equilibrium, for the end-member cases of no particles (blue lines), and no advection (orange lines). Left panels are global mean, others are from locations in Figure 4. If there were no particles, the Hg concentration would be homogenized throughout the ocean by the circulation. If there were no circulation, the concentration in the steady state increases with depth in the ocean, because there are fewer sinking particles at depth, so the Hg abundance per particle has to increase, as does therefore the dissolved Hg concentration in the ocean.

Deleted: ... [50]

david archer 8/21/2018 8:55 AM

Deleted: line), and no advection (orange line).

david archer 8/21/2018 8:55 AM

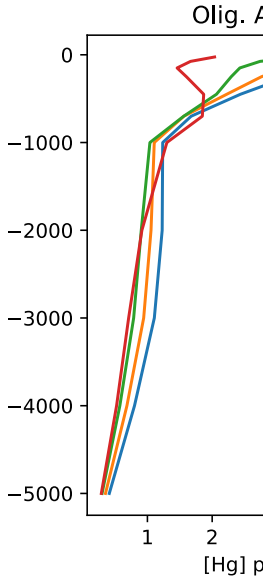

Deleted:

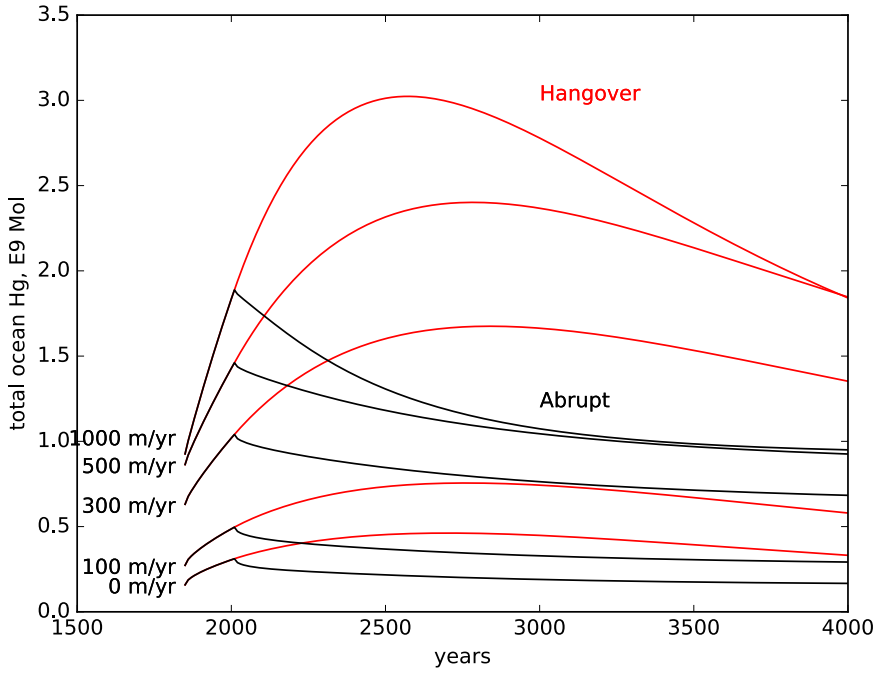

Figure 9. Time series of the ocean load of Hg (Mmol), in response to 250 years of enhanced Hg(II) deposition (1850-2100), followed by abrupt return to natural Hg deposition rates, or 1000-year wind-down in anthropogenic deposition due to recycling from the ocean.

david archer 8/21/2018 8:55 AM
Deleted: Profiles of the change in total Hg concentration following 230 years of enhanced anthropogenic Hg(2+) deposition, for different values of the Hg-particle sinking velocity ... [51]

david archer 8/21/2018 8:55 AM
Deleted: 230

david archer 8/21/2018 8:55 AM
Deleted: 2+)

david archer 8/21/2018 8:55 AM
Deleted: ,

david archer 8/21/2018 8:55 AM
Deleted: immediate

david archer 8/21/2018 8:55 AM

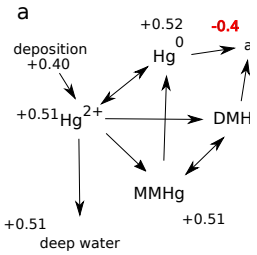

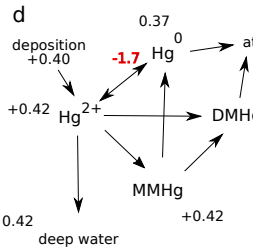

Deleted: ... [52]

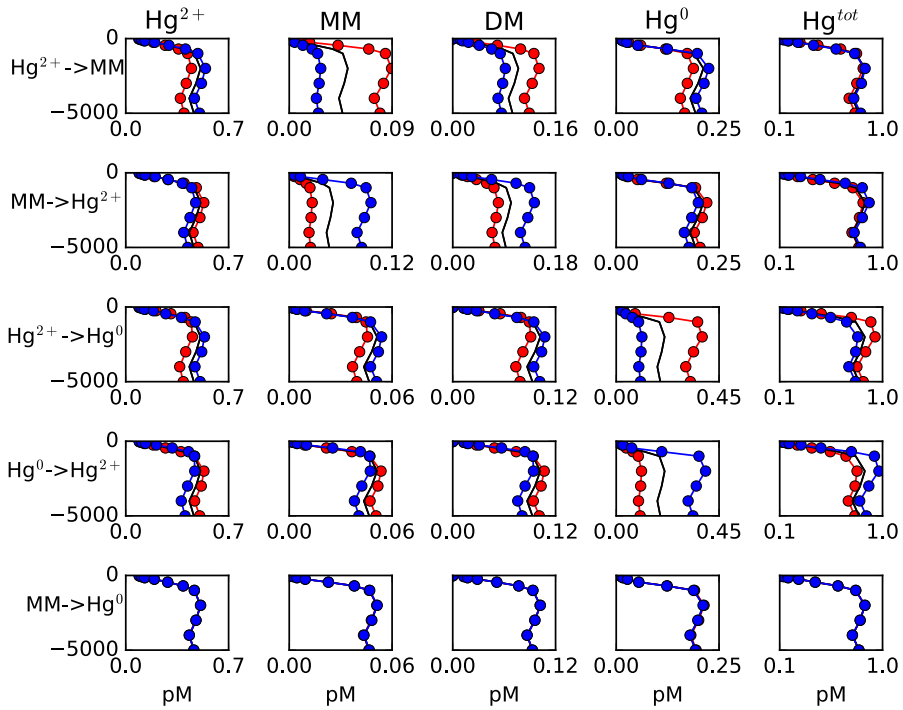

Figure 10. Model sensitivity to kinetic rate constants in the Hg system. For each kinetic rate constant printed on the left-hand side, global mean concentrations of each species are given in the four plots in that row, as indicated by the labels at the top of each column. Black lines represent the base case, and red and blue represent factors of 2 higher and lower for that kinetic rate constant, respectively.

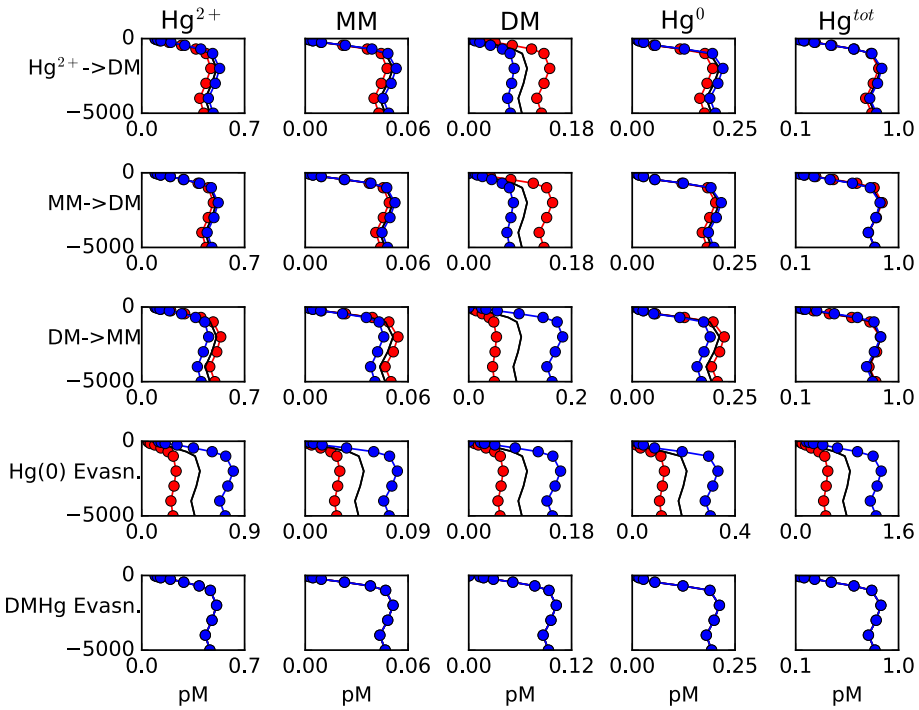

Figure 10. Continued

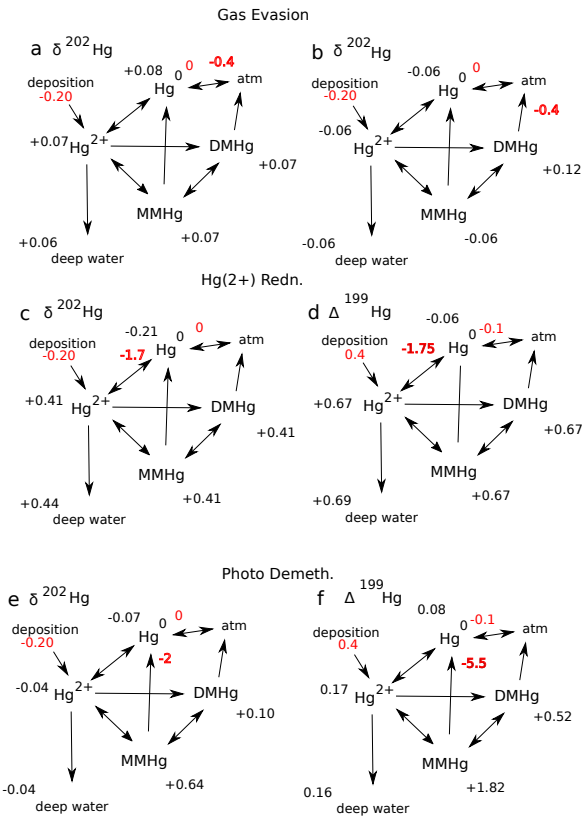

Figure 11. Schematic of the expression of isotopic fractions on the global mean sea surface isotopic signatures of the Hg species in the model, for preanthropogenic steady state. Fractionation epsilon values are shown in red, expressed as permil differences in the $^{202}Hg/^{198}Hg$ ratio. Resulting global surface average $\delta^{202}Hg$ values for each species are in black. Isotopic compositions of the wet and dry deposition are preanthropogenic estimates from Sun et al. (Sun et al., 2016) A) Mass dependent fractionation applied to Hg(0) evasion (Wiederhold et al., 2010) as the only fractionation mechanism. B) Fractionation applied to DMHg evasion (assuming the same fractionation as for Hg(0) evasion). C and D) Fractionation is applied in the reduction of Hg(II) to form Hg(0) (Kritee et al., 2007). E and F) Fractionation in biological and photo demethylation/reduction of MMHg to form Hg(0). The ε^{202} isotopic fractionation is taken to be a weighted average of biological (Kritee et al., 2007) and photochemical (Bergquist and Blum, 2007;Blum et al., 2014), while the ε^{199} is from (Bergquist and Blum, 2007). G) Fractionation of biological MMHg production from (Rodriguez-Gonzalez et al., 2009). H) Biological demethylation from (Kritee et al., 2007). I) Fractionation during adsorption of Hg(II) onto POC is from (Wiederhold et al., 2010).

Joel Blum 7/31/2018 3:21 PM
Comment [23]: d202 needs to be d202Hg and D199 needs to be D199Hg and so-on.

Joel Blum 8/4/2018 11:52 AM
Comment [24]: On the fugure you need to add Hg where=ever you have delta values.

david archer 8/21/2018 8:55 AM
Moved up [6]: Figure 11.

david archer 8/21/2018 8:55 AM
Moved (insertion) [6]

david archer 8/21/2018 8:55 AM
Deleted: Schematic of the expression of isotopic fractions on the isotopic signatures of the Hg species in the model. Fractionations are shown in red, expressed as per mille between 202 and 198. Resulting average δ^{202} values for each species are in black. A) Mass dependent fractionation applied to Hg(0) evasion (Wiederhold et al., 2010). B) applied to DM Hg degassing (assuming the same fractionation as for Hg(0) evasion). C) Both gas evasion fractionations applied simultaneously. The results in C are the sum of those in A and B. D) Fractionation is applied in the reduction of Hg(2+) to form Hg(0) (Kritee et al., 2007); E) in the methylation of Hg(2+) to form MMHg (Kritee et al., 2009); F) in demethylation / reduction of MMHg to form Hg(0). G) shows the impact of fractionation in particle adsorption. H) shows photochemical demethylation Δ^{199} MIF mass independent fractionation results, while (I) is the effect on δ^{202} from that process , using the ratio of Δ^{199} to δ^{202} that results and (i) Hg(2+) reduction. ... [53]

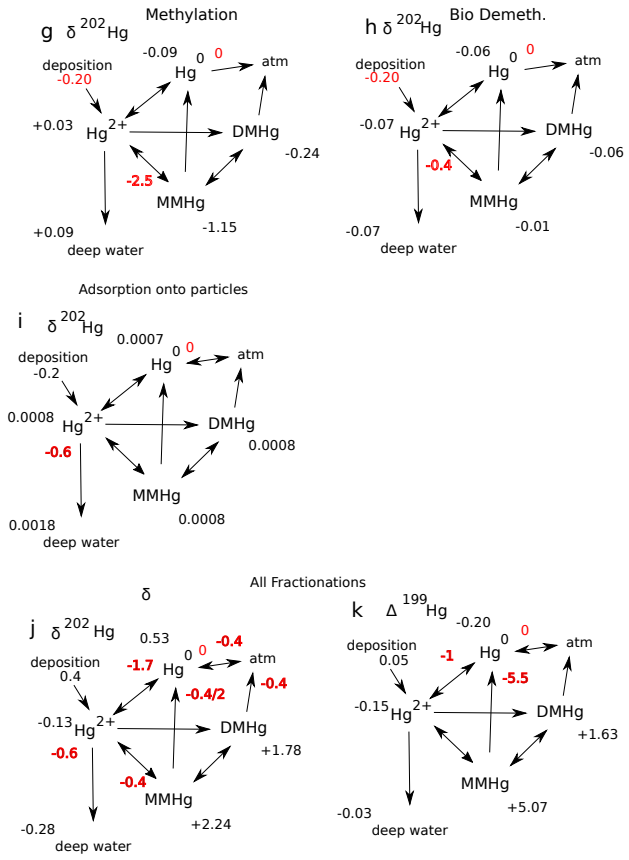

Figure 11. Continued.

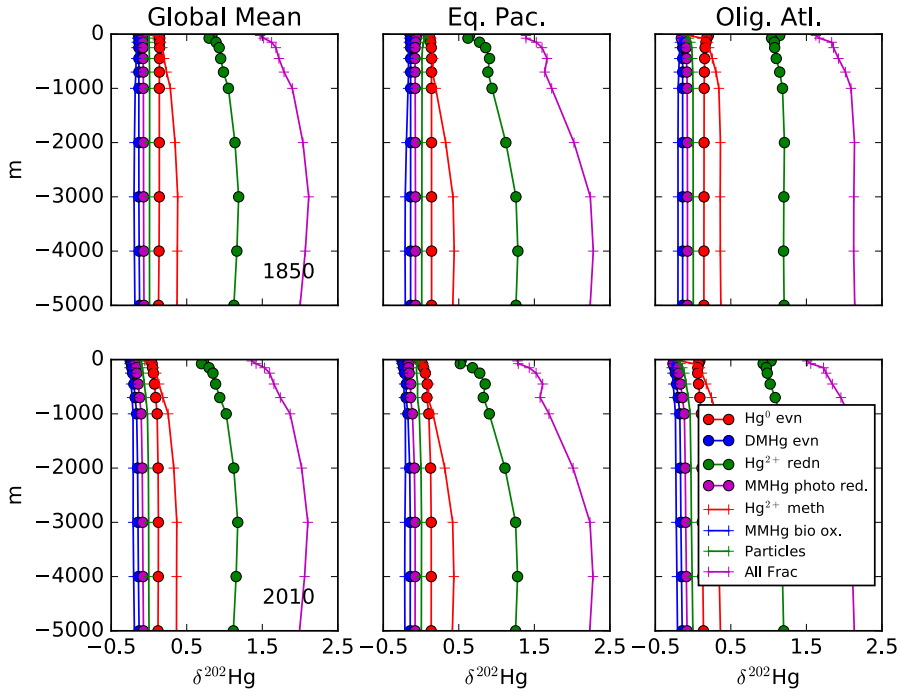

Figure 12. Profiles of δ^{202}Hg(II) and Δ^{199}Hg(II) for different fractionation scenarios, global mean, and for the locations in Figure 4.

david archer 8/21/2018 8:55 AM
Deleted: 2+)

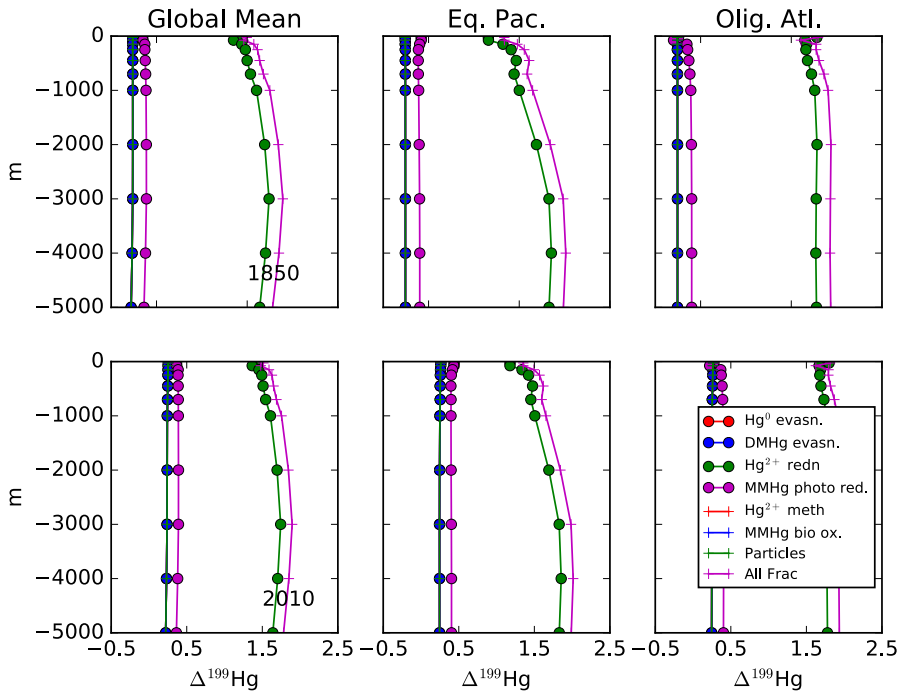

Figure 12. Continued.

david archer 8/21/2018 8:55 AM

Parti

Evas

Dark

MMH

Dark

Photo

All Fr

Deleted:

david archer 8/21/2018 8:55 AM

Deleted: 13

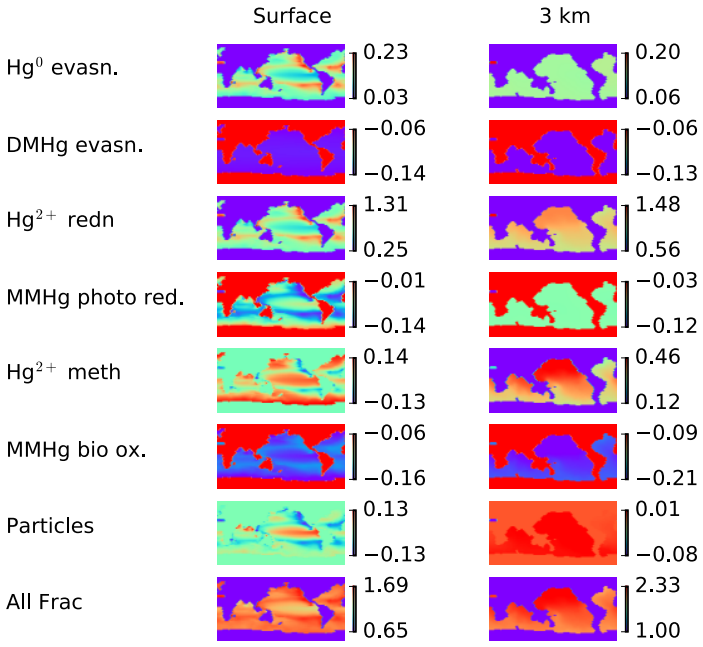

Figure 13a. Maps of δ^{202}Hg(II) at the sea surface (left) and at 3 km depth (right) for different fractionation scenarios.

david archer 8/21/2018 8:55 AM
Deleted: 2+)

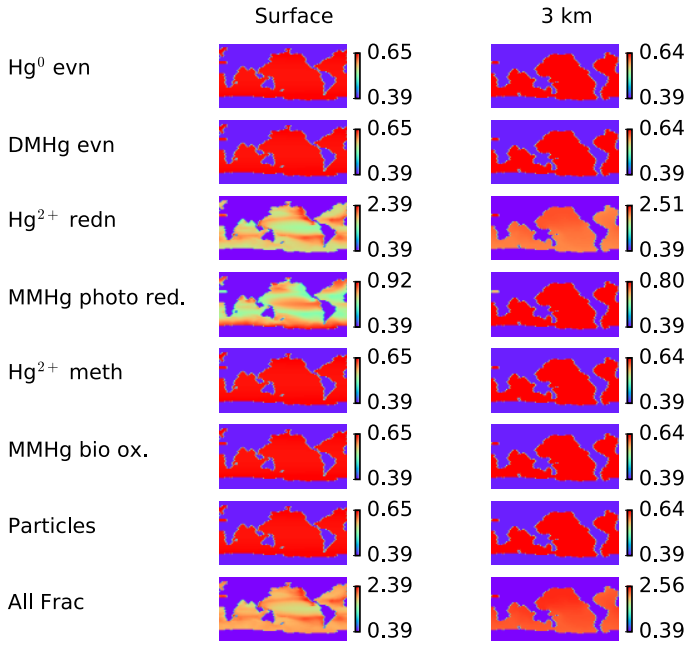

Figure 13b. Maps of Δ^{199}Hg(II) at the sea surface (left) and at 3 km depth (right) for different fractionation scenarios.

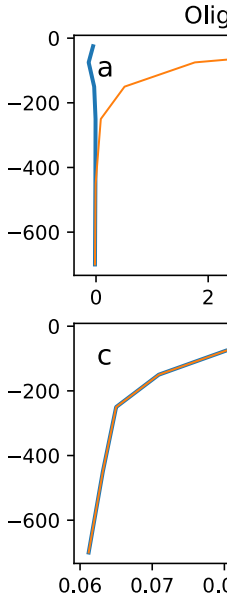

Deleted:

david archer 8/21/2018 8:55 AM

Moved down [7]: ... [54]

david archer 8/21/2018 8:55 AM

Deleted: Profiles of Δ^{199} of MMHg for th ... [55]

david archer 8/21/2018 8:55 AM

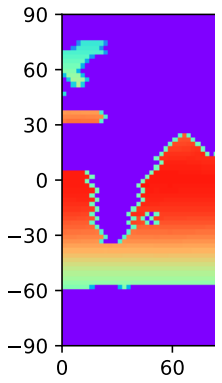

Deleted:

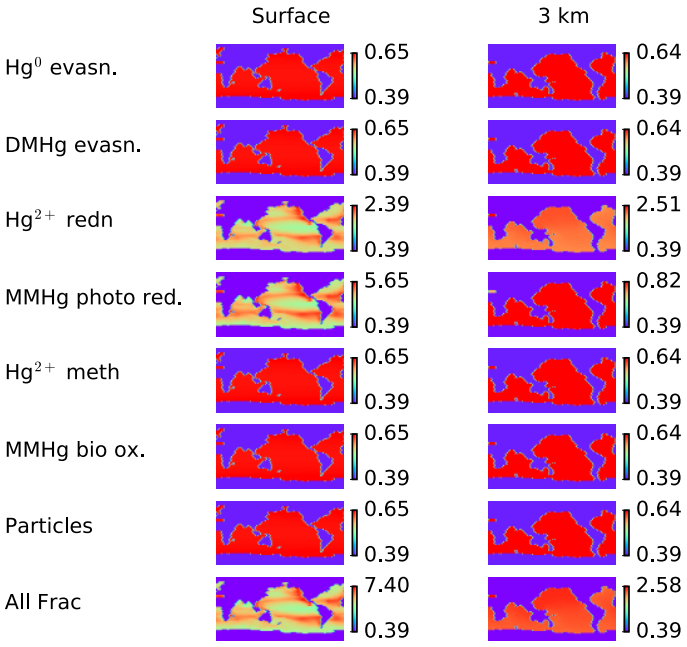

Figure 13c. Maps of Δ^{199}Hg of MMHg at the sea surface (left) and at 3 km depth (right) for different fractionation scenarios.

david archer 8/21/2018 8:55 AM
Moved down [8]: Figure 15.

david archer 8/21/2018 8:55 AM
Deleted: A map

david archer 8/21/2018 8:55 AM
Deleted: sea surface Δ^{199}

david archer 8/21/2018 8:55 AM
Deleted: showing a latitudinal dependence due to

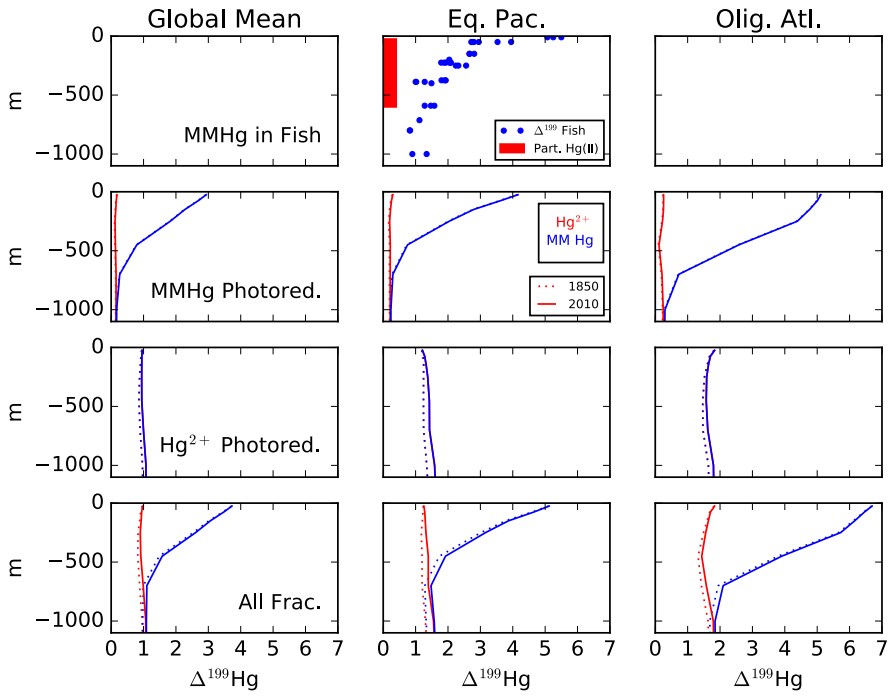

Figure 14. Profiles of Δ^{199}Hg of MMHg and Hg(II) for photochemical fractionation mechanisms. Top row is observations of MMHg Δ^{199}Hg inferred from measurements of fish (Blum et al., 2013, and Δ199Hg for Hg(II) from measurements of Hg on particles [Motta LC, submitted #6704). Second row shows model results with MMHg photoreduction, using isotope fractionation from (Bergquist and Blum, 2007). Third row shows the impact of Hg(II) photo reduction (Kritee et al., 2007). Bottom row shows sum of MMHg and Hg(II) photo reduction mechanisms. Locations for the Eq. Pac. and Olig. Atl. profiles are given in Figure 4.

david archer 8/21/2018 8:55 AM
Moved (insertion) [7]

david archer 8/21/2018 8:55 AM
Formatted: Normal

Joel Blum 8/4/2018 12:04 PM
Comment [25]: add Hg after 199 in the figure itelf

david archer 8/21/2018 8:55 AM
Deleted: intensity

david archer 8/21/2018 8:55 AM
Deleted: sunlight driving

david archer 8/21/2018 8:55 AM
Deleted: reactions

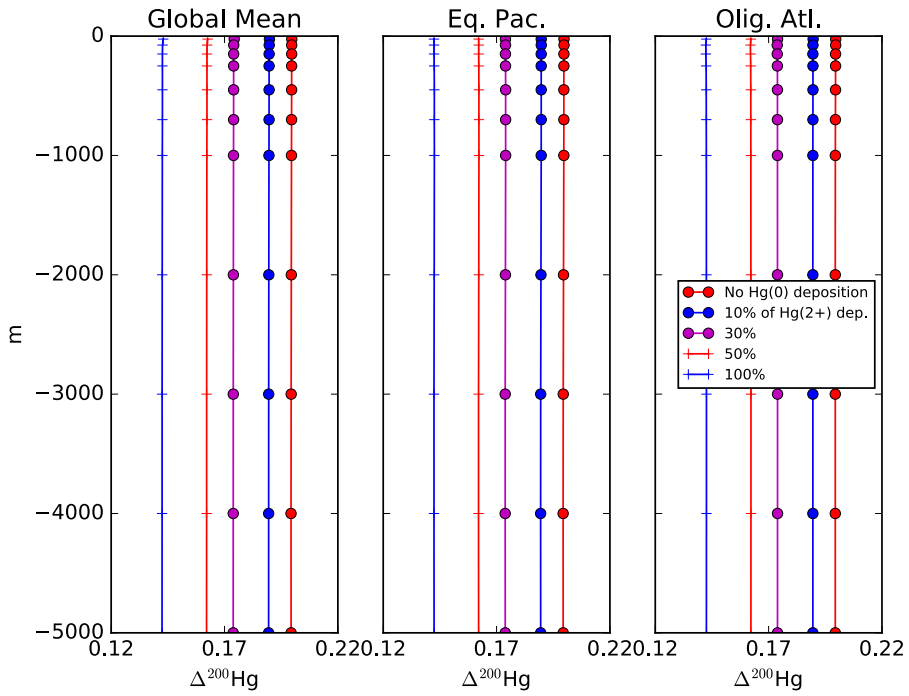

Figure 15. Profiles of the Δ^{200}Hg isotopic composition of Hg(II) for different values of the dry deposition (Hg(0)) flux. The rate of wet deposition is the same for all runs. Locations for the Eq. Pac. and Olig. Atl. profiles are given in Figure 4.

david archer 8/21/2018 8:55 AM
Moved (insertion) [8]

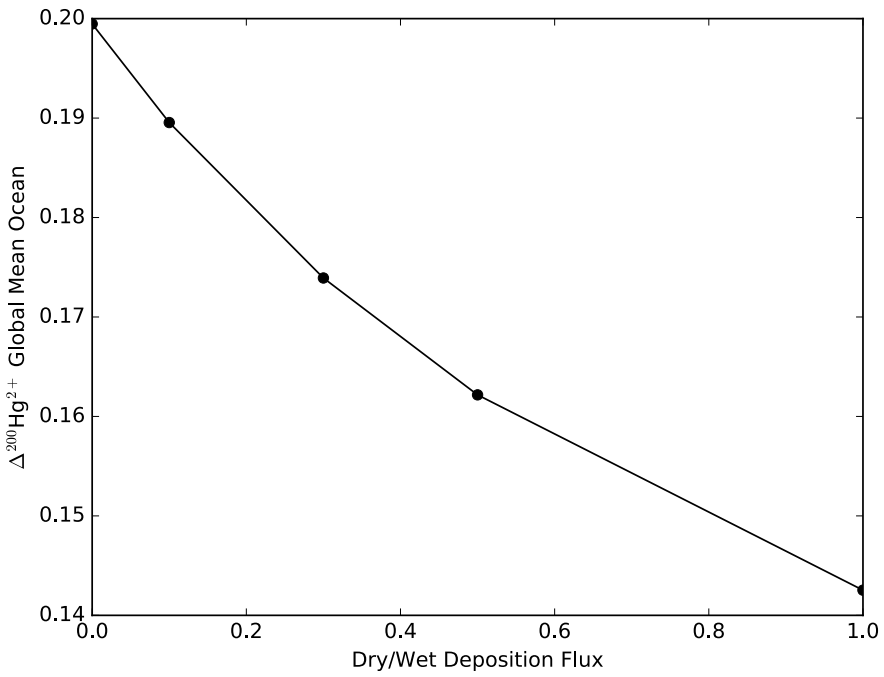

Figure 16. The Δ^{200}Hg isotopic composition of the global mean ocean is a function of the ratio of wet and dry deposition fluxes.

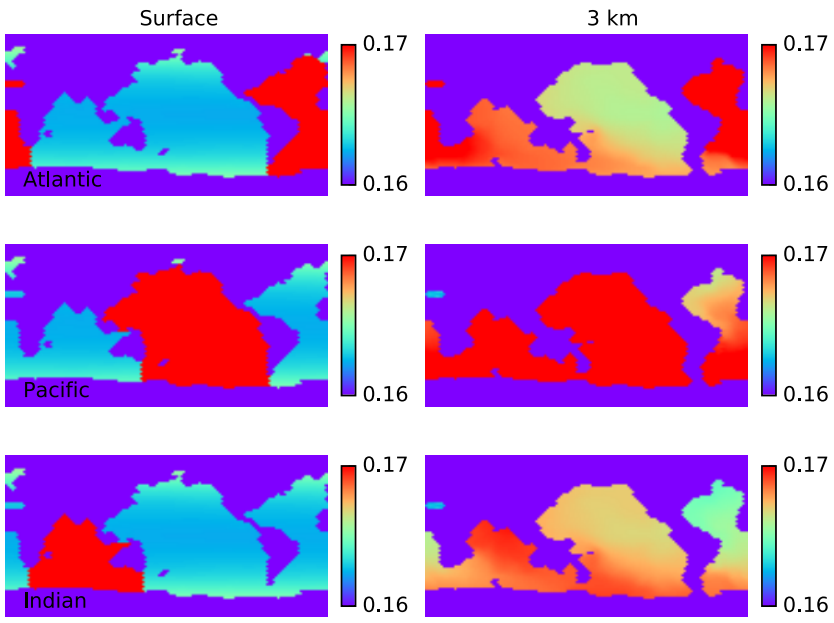

Figure 17. Maps of steady-state distribution of Δ^{200}Hg(II) under conditions of a doubling of the Hg(II) deposition flux which is isolated to the Atlantic, Pacific, and Indian oceans. The isotopic signature at 3 km depth reflects differences in surface deposition.